



**HAL**  
open science

## Layer-stacking irregularities in C36-type Nb-Cr and Ti-Cr Laves phases and their relation with polytypic phase transformations

Jochen Aufrecht, Wolfgang Baumann, Andreas Leineweber, Viola Duppel,  
Eric Jan Mittemeijer

► **To cite this version:**

Jochen Aufrecht, Wolfgang Baumann, Andreas Leineweber, Viola Duppel, Eric Jan Mittemeijer. Layer-stacking irregularities in C36-type Nb-Cr and Ti-Cr Laves phases and their relation with polytypic phase transformations. *Philosophical Magazine*, 2010, 90 (23), pp.3149-3175. 10.1080/14786435.2010.482068 . hal-00602595

**HAL Id: hal-00602595**

**<https://hal.science/hal-00602595>**

Submitted on 23 Jun 2011

**HAL** is a multi-disciplinary open access archive for the deposit and dissemination of scientific research documents, whether they are published or not. The documents may come from teaching and research institutions in France or abroad, or from public or private research centers.

L'archive ouverte pluridisciplinaire **HAL**, est destinée au dépôt et à la diffusion de documents scientifiques de niveau recherche, publiés ou non, émanant des établissements d'enseignement et de recherche français ou étrangers, des laboratoires publics ou privés.



**Layer-stacking irregularities in C36-type Nb-Cr and Ti-Cr Laves phases and their relation with polytypic phase transformations**

Journal:	<i>Philosophical Magazine &amp; Philosophical Magazine Letters</i>
Manuscript ID:	TPHM-10-Jan-0014.R1
Journal Selection:	Philosophical Magazine
Date Submitted by the Author:	17-Mar-2010
Complete List of Authors:	Aufrecht, Jochen; Max Planck Institute for Metals Research Baumann, Wolfgang; Max Planck Institute for Metals Research, Prof. Dr Ir. E.J. Mittemeijer Leineweber, Andreas; Max Planck Institute for Metals Research, Department Mittemeijer Duppel, Viola; Max Planck Institut for Solid State Research Mittemeijer, Eric Jan; Max Planck Institute for Metals Research, Prof. Dr Ir. E.J. Mittemeijer; University of Stuttgart, Institute for Materials Science
Keywords:	intermetallics, phase transformations, phase transitions, TEM, X-ray diffraction, crystal structure, crystal defects, HRTEM
Keywords (user supplied):	line-broadening analysis



# Layer-stacking irregularities in C36-type Nb-Cr and Ti-Cr Laves phases and their relation with polytypic phase transformations

J. Aufrecht<sup>1</sup>, W. Baumann<sup>1</sup>, A. Leineweber<sup>1</sup>, V. Duppel<sup>2</sup>, E. J. Mittemeijer<sup>1,3</sup>

<sup>1</sup>Max Planck Institute for Metals Research, Heisenbergstr. 3, D-70569 Stuttgart, Germany

<sup>2</sup>Max Planck Institute for Solid State Research, Heisenbergstr. 1, D-70569, Stuttgart, Germany

<sup>3</sup>Institute for Materials Science, University of Stuttgart, Heisenbergstr. 3, D-70569 Stuttgart, Germany

## Abstract:

Specific layer-stacking irregularities have been identified in C36 (4H) Nb-Cr and Ti-Cr Laves-phases on the basis of X-ray diffraction line-profile analysis and high resolution transmission-electron microscopy. Domain boundaries and transformation errors within domains could be distinguished. The layer-stacking irregularities in both C36-NbCr<sub>2</sub> and C36-TiCr<sub>2</sub> can be associated with a preceding C14 (2H) → C36 (4H) phase transformation carried out by glide of mobile synchro-Shockley partial dislocation dipoles in an ordered fashion. The stacking irregularities observed can be interpreted as deviations from such perfect “ordered glide”. The interpretation is supported by the observation that in case of C36-NbCo<sub>2</sub>, where no preceding C14 → C36 transformation occurs, different layer-stacking irregularities are observed.

## 1. Introduction

### 1.1 Laves phases; layer-stacking rules

In the last ten years the interest in Laves phases (general formula  $AB_2$ ;  $A, B$ : metal atoms) has grown pronouncedly. From a practical point of view, Laves phases have been proposed as candidates for structural materials, but also for functional materials, like magnetic, superconducting materials and as hydrogen-storage materials [1]. From a scientific point of view, the Laves phases constitute the largest group of intermetallic phases occurring in a very large number of binary and ternary systems [2, 3], which makes it possible to study specific properties as function of the elemental constituents of

1  
2  
3 the Laves phase. Such information allows tailoring the properties for specific  
4 applications.  
5

6  
7 Laves phases are characterised by their specific crystal structures, which are  
8 tetrahedrally close-packed structures and thus belong to the so-called Frank-Kasper  
9 phases [4, 5]. The different Laves-phase crystal-structure types can be conceived as  
10 polytypes generated by stacking several types of atomic layers subject to some particular  
11 stacking principles (Fig. 1). These crystal structures imply that the atomic-radius ratio of  
12 the *A* and *B* atoms,  $r_A/r_B$ , equals  $(3/2)^{1/2} \approx 1.225$ , regarding the atoms as hard spheres.  
13  
14

15  
16 Different descriptions of stacking rules leading to the Laves phases are available in  
17 the literature. For the current purposes it suffices to focus on the stacking of *layer-*  
18 *sandwich units*, each composed of a specific stack of three atomic layers,  $AB_3A$  (this  
19 notation refers to the composition of this stacking unit; called layer triplets in Ref. [6];  
20 not identical with the triple layers considered in some other works [7, 8]). Between these  
21 layer-sandwich units additional *single-layer units*, *B* are located (see Fig. 1). With respect  
22 to a given two-dimensional hexagonal unit mesh defined by the lattice-structure basis  
23 vectors **a** and **b** perpendicular to the stacking direction, the *A* atoms of the *layer-sandwich*  
24 *units* and the *B* atoms of the *single-layer units* can each assume three different relative  
25 positions, i.e. at fractional coordinates either (0, 0), or (1/3, 2/3) or (2/3, 1/3).<sup>1</sup>  
26 Representing the position of the layer-sandwich units by X, Y, and Z, and of the single-  
27 layer units by x, y, and z, depending on which of the former three positions is assumed by  
28 the layer concerned (i.e. (0, 0): X, x; (1/3, 2/3): Y, y; and (2/3, 1/3): Z, z), the layer-  
29 stacking sequence of a Laves phase can be represented by an alternate sequence of these  
30 upper- and lower-case letters. The following rules apply additionally:  
31  
32

33  
34 (i) Taking first only into account the upper-case letters, a given letter, say X, may only be  
35 followed by a different other upper-case letter, in this case Y or Z, i.e. an X cannot be  
36 followed by an X (Y not by Y; Z not by Z).  
37

38  
39 (ii) A *single-layer unit* located between two *layer-sandwich units* is represented by a  
40 lower-case letter different from the upper-case letters representing the adjacent *layer-*  
41 *sandwich units*.  
42  
43

44  
45  
46  
47  
48  
49  
50  
51  
52  
53  
54  
55  
56  
57 <sup>1</sup>Use of the symbols A, B, and C to indicate the relative layer positions is prevented to avoid confusion with  
58 the symbols A and B used for the two different metals constituting the Laves phase  $AB_2$ .  
59  
60

*sandwich units*. Consequently, a z-type single layer is located between X and Y, i.e. the corresponding part of the stacking sequence reads ...XzY.. or ..YzX...

Since the positions of the single layer units are unambiguously prescribed by the positions of the adjacent layer-sandwich units (see above), it is sufficient for most purposes to consider only the upper-case letters to indicate the stacking sequence, as done at most places in the present paper. In terms of only the X, Y, and Z symbols describing the stacking sequences following the rules given above, the possible polytypes of Laves phases constitute one-to-one analogues of the polytypes possible for closed-packed structures of pure elements, and also of the polytypes possible for SiC, CdI<sub>2</sub> etc. Against this background, see also Table 1 summarizing the most important Laves-phase polytypes.

Table 1: The most important Laves-phase stacking types described as polytypes (see text)

stacking sequence	stacking sequence, "reduced"	Jagodzinski symbol <sup>a</sup> [9]	Ramsdell symbol [10]	Strukturbericht symbol [11]	prototype	space group
XzYxZy	XYZ	c	3C	C15	MgCu <sub>2</sub>	$Fd\bar{3}m$
XzYz	XY	h	2H	C14	MgZn <sub>2</sub>	$P6_3/mmc$
XzYxZxYz	XYZY	ch	4H	C36	MgNi <sub>2</sub>	$P6_3/mmc$
XzYxZyXyZxYz	XYZXZY	cch	6H <sup>b</sup>	--	--	$P6_3/mmc$

<sup>a</sup> The Jagodzinski symbol indicates the stacking transition associated with a certain layer-sandwich unit: "h", if the layer-sandwich units above and below the respective layer are both at the same position and "c" if they are at different positions. The respective crystal structures are built up by infinite repetition of the stacking transitions given by the Jagodzinski symbols. To obtain one single, complete unit cell in stacking direction of the respective crystal structure, the number of layers given by the Ramsdell symbol is necessary; i.e. ...ccc... for 3C, ...hh... for 2H, ...chch... for 4H and ...cchcch... for 6H.

<sup>b</sup>This 6H-type structure is often referred to as 6H<sub>1</sub>. The 6H<sub>2</sub> structure with the Jagodzinski symbol hchhc is not considered here.

## 1.2 Partial-dislocation dipole mechanism for polymorphic transformations in Laves phases

The phase diagrams of many binary and ternary systems comprise several Laves-phase polytypes. The stability of a particular polytype can vary as function of composition or temperature (at constant pressure). A transformation from one to another polytype is in principle possible without need of long-range diffusion. A number of works have been dedicated in the past to the problem how such a polymorphic transformation can occur [12, 13, 14, 7, 8]. One main idea is that the layer-stacking sequences, considering only the layer-sandwich units, are changed by glide of partial dislocations, with six different Burgers vectors  $\pm\mathbf{b}_1 = \pm\frac{1}{3}[10\bar{1}0]$ ,  $\pm\mathbf{b}_2 = \pm\frac{1}{3}[\bar{1}100]$ , and  $\pm\mathbf{b}_3 = \pm\frac{1}{3}[0\bar{1}10]$  (Fig. 2; employing Miller-Bravais indices for hexagonal crystal structure lattices, where the basis vectors  $\mathbf{a}$  and  $\mathbf{b}$  correspond to those used for the unit mesh mentioned in section 1.1; cf. Fig.1), along the basal (0001) plane between two (assumedly rigid) *layer-sandwich units*. Thereby the relative position of the layer-sandwich unit, say “above” the (0001) glide plane becomes changed with respect to that of the layer-sandwich unit “below” the (0001) glide plane (Fig. 3). Note that, as consequence of stacking rule (ii) indicated above, this glide process requires that the *single-layer unit* between the two *layer-sandwich units* has to move synchronously in another direction, but also within the glide plane. Thus the shear process associated with one of the above-mentioned Burgers vectors is actually a synchroshear process, which has been discussed in more detail elsewhere [7, 8, 15]. The corresponding *partial dislocations* are, therefore, called synchro-Shockley partial dislocations [15].

It has been proposed [14, 15], supported by some experimental evidence (see below) that, in case of a C14 (2H)  $\rightarrow$  C36 (4H) transformation, such synchro-Shockley partial dislocations as described above do not glide through the crystal independently. Instead they glide as *dislocation dipoles*, where the two dislocations comprising the dipole have Burgers vectors of opposite sign (e.g.  $\mathbf{b}_1$  and  $-\mathbf{b}_1$ ) and with one dislocation travelling above and one dislocation travelling below a given *layer-sandwich unit*. As net effect, only the middle layer-sandwich unit and the two adjacent single layer units are shifted with respect to the initial stacking sequence, whereas the upper layer-sandwich unit

1  
2  
3  
4  
5  
6  
7  
8  
9  
10  
11  
12  
13  
14  
15  
16  
17  
18  
19  
20  
21  
22  
23  
24  
25  
26  
27  
28  
29  
30  
31  
32  
33  
34  
35  
36  
37  
38  
39  
40  
41  
42  
43  
44  
45  
46  
47  
48  
49  
50  
51  
52  
53  
54  
55  
56  
57  
58  
59  
60

remains at its original position. Hence, glide of such dislocation dipoles does not lead to a macroscopic shear of the crystal (see Fig. 4) and thus can occur under the constraint of conservation of shape of the crystal. Thus, simple, ordered (i.e. periodic) sequences of such dislocation dipoles can bring about the 2H (C14)  $\rightarrow$  4H (C36) (Fig. 5) and the 2H (C14)  $\rightarrow$  6H transformation, which have been frequently observed in real systems. Early high-resolution electron microscopy (HRTEM) studies on  $\text{TiCr}_2$ , in which a C14  $\rightarrow$  C36 transformation proceeds, revealed C36 domains growing parallel to the (0001) plane into the C14 matrix [13]. This observation is compatible with the glide of synchro-Shockley partial dislocation dipoles as transformation mechanism. In the same work [13] it was indicated that the apparent sluggishness of formation of 3C (C15)- $\text{TiCr}_2$  from 2H (C14)- $\text{TiCr}_2$  (in contrast to that of formation of 4H and also 6H) might be ascribed to the impossibility to accomplish the 2H  $\rightarrow$  3C transformation by a partial dislocation dipole mechanism as discussed above; the 2H  $\rightarrow$  3C transformation has to involve macroscopic shear for the crystal considered, which can be difficult to realize in a polycrystalline specimen.

In the present publication layer faulting in three C36-type Laves phases ( $\text{NbCr}_2$ ,  $\text{TiCr}_2$ ,  $\text{NbCo}_2$ ; see the phase diagrams provided by Fig. 6) have been studied by transmission electron microscopy and X-ray powder diffraction. It was found that the investigated C36- $\text{NbCr}_2$  and C36- $\text{TiCr}_2$  Laves phases contain specific stacking irregularities. These are compatible with the occurrence of specific irregularities in the periodic passage of the synchro-Shockley partial dislocation dipoles in the course of the 2H (C14)  $\rightarrow$  4H (C36) transformation, experienced by the  $\text{NbCr}_2$  and  $\text{TiCr}_2$  specimens. In contrast with these observations, the C36- $\text{NbCo}_2$  Laves phase does not contain such layer-stacking faults: a 2H (C14)  $\rightarrow$  4H (C36) transformation does not occur during formation of C36- $\text{NbCo}_2$  (cf. Fig. 6c).

### 1.3 Diffraction from layered hexagonal structures containing stacking irregularities

The effect of a stacking irregularity like a single stacking fault, and also of a combination of stacking faults, in a layered structure on its diffraction pattern can be understood as follows: a single stacking irregularity separates two halves of a crystal (Fig. 7). Then the unit cells of the one half of the crystal with respect to the other half may be shifted by a

1  
2  
3  
4  
5  
6  
7  
8  
9  
10  
11  
12  
13  
14  
15  
16  
17  
18  
19  
20  
21  
22  
23  
24  
25  
26  
27  
28  
29  
30  
31  
32  
33  
34  
35  
36  
37  
38  
39  
40  
41  
42  
43  
44  
45  
46  
47  
48  
49  
50  
51  
52  
53  
54  
55  
56  
57  
58  
59  
60

*displacement vector*  $\Delta\mathbf{r} = u'\mathbf{a} + v'\mathbf{b} + w'\mathbf{c}$  with, in general, real-valued  $u'$ ,  $v'$ , and  $w'$ , and  $\mathbf{a}$ ,  $\mathbf{b}$ ,  $\mathbf{c}$  as the basis vectors of the translation lattice. Non-integer  $u'$ ,  $v'$  and  $w'$  imply that for certain (some, all or most) diffraction vectors  $\mathbf{g} = h\mathbf{a}^* + k\mathbf{b}^* + l\mathbf{c}^*$ , with  $h$ ,  $k$  and  $l$  as integer-valued Miller (actually Laue) indices and  $\mathbf{a}^*$ ,  $\mathbf{b}^*$  and  $\mathbf{c}^*$  as the reciprocal basis vectors of the crystal, a phase shift occurs between the diffraction waves emanating from the two halves of the crystal. This phase shift can be shown to amount to  $2\pi\mathbf{g}\cdot\Delta\mathbf{r} = 2\pi(u'h + v'k + w'l)$ . No phase shift will occur for certain  $hkl$  if  $\mathbf{g}\cdot\Delta\mathbf{r} = u'h + v'k + w'l$  assumes an integer value, and thus the reflections pertaining to these  $hkl$  do not broaden and do not shift (in reciprocal space). For a start, the absence of other line-broadening contributions is assumed. If  $\mathbf{g}\cdot\Delta\mathbf{r}$  assumes an arbitrary, non-integer value, the otherwise delta-function shaped diffraction peak gets broadened and possibly shifted in reciprocal space into a direction perpendicular to the fault plane. For predicting how such broadening in reciprocal space will show up in an (X-ray) powder-diffraction pattern, it has to be considered that the line broadening in reciprocal space then gets projected onto the diffraction vector. For example, considering one crystal, if the stacking direction is parallel to  $\mathbf{c}^*$  and thus the fault plane is perpendicular to  $\mathbf{c}^*$ , the line broadening in reciprocal space leads to a large line broadening in the X-ray diffractogram if  $\mathbf{g} \parallel \mathbf{c}^*$ . If  $\mathbf{g} \perp \mathbf{c}^*$ , no line broadening in the X-ray diffractogram results.

The actual line broadening in case of a polycrystal or powder containing many stacking faults will depend on the probability distribution of the different types of faults. Corresponding calculations have been performed for many types of layered structures, and computer programs are available to predict for general layered structures the layer-fault induced line broadening [16]. The line broadening (and the line shift) depends on the relative phases of the diffracted waves emanating from the two crystal parts separated by a stacking irregularity. Thus, for the Laves-phase crystal structures considered here, it suffices to refer to previously worked out predictions on line broadening in similar layered crystal structures in which same types of displacement vectors occur upon varying the layer-stacking sequence. For 4H-type structures, as the C36-type Laves phase with its XYXZ stacking sequence, such results have been presented in Refs. [17, 18]. The different types of stacking faults considered in these works can be ascribed to only five types of displacement vector  $\Delta\mathbf{r}$ , which are indicated in the following by its coefficients

$(u', v', w')$ :  $\pm(0, 0, 1/4)$ ,  $(0, 0, 1/2)$ ,  $\pm(1/3, 2/3, 0)$ ,  $\pm(1/3, 2/3, \pm 1/4)$ ,  $\pm(1/3, 2/3, 1/2)$ ; see Fig. 7. Because of the translational symmetry of the crystals, all components  $u'$ ,  $v'$ ,  $w'$  of  $\Delta\mathbf{r}$  are equivalent to  $u' \bmod 1$ ,  $v' \bmod 1$  and  $w' \bmod 1$ , respectively. The occurrence of one of these displacement vectors leads to a specific characteristic  $hkl$  dependence of the line broadening (and the line shift) in reciprocal space. The  $hkl$  dependence of the line broadening can be systematised by considering six classes of  $hkl$  reflections, depending on the values of  $h - k$  and of  $l$ . Of these classes, one with  $h - k = 3N$  and  $l = 4M$  (with integer  $N, M$ ) shows no line broadening for any of the five  $\Delta\mathbf{r}$ . Two further classes, with  $h - k = 3N$  and  $l = 4M \pm 1$ , and with  $h - k = 3N$  and  $l = 4M + 2$ , are irrelevant because their reflections have an integrated intensity of exactly or close to 0 (these classes were not considered explicitly in Refs. [17, 18]). Three further classes show line broadening characteristic for the corresponding type of  $\Delta\mathbf{r}$ , see Table 2. Note that the appearance of a "0" in a cell in Table 2 means that the reflections of that reflection class remain unbroadened for the type of displacement vector considered, which implies that  $\mathbf{g} \cdot \Delta\mathbf{r} = u'h + v'k + w'l$  is an integer.

Table 2. Extent of line broadening for a 4H-type crystal (as C36) along  $\mathbf{c}^*$  in reciprocal space as function of the displacement vector for four of the six reflection classes<sup>a</sup>. The width in reciprocal space units (here not specified) is proportional to the indicated numbers, as well as to the specimen-dependent probability for the occurrence of the corresponding displacement vectors.  $N$  and  $M$  are integers.

reflection-class; conditions for $hkl$	displacement vector, $\Delta\mathbf{r} = (u', v', w')$				
		$\pm(0,0, 1/4)$	$(0, 0, 1/2)$	$\pm(1/3, 2/3, 0)$	$\pm(1/3, 2/3, \pm 1/4)$
$h - k = 3N$ $l = 4M$	0	0	0	0	0

$h - k \neq 3N$ $l = 4M$	0	0	3	3	3
$h - k \neq 3N$ $l = 4M \pm 1$	2	4	3	2	1
$h - k \neq 3N$ $l = 4M + 2$	4	0	3	1	3

a) The two additional reflection classes indicated by  $h - k = 3N$  and  $l = 4M \pm 1$ , and  $h - k = 3N$  and  $l = 4M + 2$  are irrelevant due to the zero or negligible integrated intensity of the corresponding  $hkl$  reflections.

## 2. Experimental

### 2.1 Preparation of alloys

The NbCr<sub>2</sub> (target composition 34.5 at.% Nb) and the TiCr<sub>2</sub> (target composition 35.8 at.% Ti) alloys were prepared by arc melting high-purity metals (niobium 99.99 wt%, titanium 99.999 wt%; chromium 99.999 wt%) under a titanium-gettered argon atmosphere. To ensure chemical homogeneity, the samples were flipped, remelted and subsequently cooled down on a water-cooled copper hearth for several times. Although samples of various compositions were prepared, the observations presented here were found to be composition-independent and can be discussed by considering, exemplarily, specimens of the two compositions indicated above.

The NbCr<sub>2</sub> ingot was used as obtained after arc-melting because C36 material can only be obtained in as-cast conditions [19]. The TiCr<sub>2</sub> ingot was subjected to further heat treatments. First, the sample was annealed for 50 h at 1395 °C (in the bcc-solid solution region; cf. Fig. 6b) to ensure chemical homogeneity, i.e. to eliminate the chemical inhomogeneity inherent to the dendritic as-cast structure. Thereafter, the specimen was annealed for 50 h at 1200 °C (in the C36 Laves-phase region; cf. Fig. 6b). These heat treatments were carried out in an induction furnace under a high-purity argon atmosphere. To this end, the sample was placed into an Y<sub>2</sub>O<sub>3</sub> crucible which was covered with three Ti-getter sheets. Before starting the annealing the furnace was evacuated and back-filled with argon for several times. After the annealing, the specimens were rapidly cooled down by switching off the furnace.

1  
2  
3 Preparation of the C36-type Nb-Co Laves phase (25.0 at.% Nb) powder, has been  
4 described in Ref. [20]. Note that this material has been considered here on the sole basis  
5 of its X-ray powder diffraction pattern.  
6  
7

8 Both the as-cast NbCr<sub>2</sub> alloy and the as-cast and heat treated TiCr<sub>2</sub> alloy were  
9 characterised by optical microscopy, scanning electron microscopy (SEM), and  
10 energy/wavelength dispersive X-ray analysis (EDX/EPMA-WDX electron microprobe  
11 analysis), X-ray powder diffractometry (XRPD) and high resolution transmission-  
12 electron microscopy (HRTEM).  
13  
14

15 For the TEM and XRPD measurements powders of the NbCr<sub>2</sub> and TiCr<sub>2</sub> alloys  
16 were produced within a mortar. In case of NbCr<sub>2</sub> the material was taken from the top of  
17 the ingots containing predominantly C36 phase [19]. In case of TiCr<sub>2</sub>, for the XRPD both  
18 a fine and a coarse powder batch were produced. For the SEM and EDX/EPMA-WDX  
19 analyses metallographic cross sections were prepared which were manually ground and  
20 polished. A Cameca SX100 microprobe was employed for the EPMA-WDX  
21 measurements, applying an acceleration voltage of 15 kV and a current of 40 nA.  
22 Elemental standards (Nb, Ti, Cr) were employed for quantification according to the  $\Phi(\rho z)$   
23 approach [21]. The electron backscattering diffraction (EBSD) measurements were  
24 conducted using a Zeiss LEO 438 VP scanning electron microscope equipped with an  
25 EBSD system (TSL, EDAX, Inc.) and the software OIM 4.5.  
26  
27

28 Chemical analysis by carrier-gas hot extraction (ELTRA ONH 2000), combustion  
29 technology (ELTRA CS-800) and Inductively Coupled Plasma Optical Emission (Spectro  
30 – CIROS CCD) showed that no uptake of metallic or non-metallic impurities had  
31 occurred during sample production and treatment.  
32  
33  
34  
35  
36

## 37 **2.2 High resolution transmission electron microscopy (HRTEM)**

38 Due to the brittle nature of the investigated coarsely ground NbCr<sub>2</sub> and TiCr<sub>2</sub> powders,  
39 the edges of the powder particles were thin enough for electron transmission. The powder  
40 was suspended in n-butanol. Afterwards, a holey-carbon covered copper net was  
41 covered with that suspension leaving behind, after evaporation of the liquid, wedge-  
42 shaped crystallites in random orientation transparent for electrons. HRTEM was  
43 performed using a Philips CM 30 with an accelerating voltage of 300 kV.  
44  
45  
46  
47  
48  
49  
50  
51  
52  
53  
54  
55  
56  
57  
58  
59  
60

### 2.3 X-ray powder diffraction (XRPD)

XRPD was performed using a “Philips X`Pert MPD” diffractometer equipped with a germanium-monochromator in the incident beam, selecting Cu-K $\alpha_1$  radiation.

In case of the TiCr<sub>2</sub> powder specimen, for correction of instrumental broadening, the instrumental line-profile contributions were determined using a LaB<sub>6</sub> powder sample (NIST standard reference material, SRM660a) using TOPAS [22]. These instrumental contributions were then convoluted with pseudo-Voigt functions which were fitted to the reflections of the experimental TiCr<sub>2</sub> diffraction patterns by least squares minimization. The fitting parameters were the reflection-maximum position,  $2\theta_{\max}$  and the full width at half maximum (FWHM) of the only structurally broadened line profiles; the line-shape parameter  $\eta$  was fixed to a value of 1.2 for all reflections<sup>2</sup>. Similar fits using pseudo-Voigt functions were conducted for NbCr<sub>2</sub>, however, without separate consideration of the instrumental contribution (because of the considerably larger structural line broadening in case of NbCr<sub>2</sub>) and with  $\eta$  as an additional fit parameter.

Diffraction patterns of the Nb-Co alloy powder specimen were recorded using a Huber G670 Guinier camera equipped with an incident-beam germanium monochromator, selecting Co-K $\alpha_1$  radiation. The powder was put as a thin layer on a Kapton foil. Like for NbCr<sub>2</sub>, because of the relative large structural line broadening, without making separate consideration of the instrumental contribution, the reflection positions and widths were determined by fitting Lorentzian functions (corresponding to pseudo-Voigt functions with fixed  $\eta = 1$ ; see also footnote 2) to each reflection.

## 3. Results

### 3.1 Nb-Cr

#### 3.1.1 Phase analysis and composition

For the as-cast NbCr<sub>2</sub> specimens, a majority of crystallites of the hexagonal C36 modification occur at the top of the arc-melted ingot, together with a minor amount of

---

<sup>2</sup> Fixing the peak-shape parameter  $\eta$  to a certain, reasonable value, removes the possible correlation of the FWHM and  $\eta$  in a fitting procedure and thereby the  $hkl$  dependency of the FWHM is more clearly exhibited. This procedure was necessary for the TiCr<sub>2</sub> powder specimen and for also the Nb-Co alloy powder specimen.

1  
2  
3 (retained; cf. Fig. 6a) hexagonal C14-type crystallites (see Fig. 10a) and cubic C15 type  
4 crystallites [19]. The bottom part of the ingot mainly consists of the C15 modification.  
5 Recent research performed in the present project has demonstrated that the C14 and C36  
6 modifications are metastable at all temperatures and form only upon solidification from  
7 the melt at the top of the initially arc-melted ingots, with the C36 phase forming by solid  
8 state transformation from the initially crystallized C14 (see Refs. [19, 23]). The powder  
9 used for the present study was taken from the top of the arc-melted ingot (cf. section 2.1).  
10 Because, in order to maintain the C36 modification, the sample could not be  
11 homogenized rigorously (this would have led to transformation of the C14/C36  
12 crystallites to C15; cf. Fig. 6a) compositional inhomogeneities as a result of the  
13 solidification process are possible. The average niobium content of the sample was  
14 determined by WDX-EPMA to be equal to  $34.9 \pm 0.2$  at.%. A niobium content somewhat  
15 higher than the target composition (34.5 at.%) can be ascribed to chromium evaporation  
16 during arc-melting.  
17  
18  
19  
20  
21  
22  
23  
24  
25  
26  
27  
28  
29

### 30 3.1.2 XRPD

31 Although the powder taken from the top part of the as-cast specimen contains C14-  
32 and C15-type crystallites additional to the C36 majority phase crystallites (cf. section  
33 3.1.1), separate reflections of these minority phases are not visible in the X-ray  
34 diffraction pattern (Fig. 8a) because they are superimposed on the C36 reflections  
35 occurring at the same values of the diffraction vector  $Q$ . In view of the tiny amounts of  
36 C14 and C15 phase, for the current purpose the diffraction patterns can yet be conceived  
37 as characteristic for the C36 phase.  
38  
39  
40  
41  
42  
43

44 The recorded diffraction pattern exhibits a distinct  $hkl$ -dependent broadening of  
45 reflections: The broadening occurs for (and is restricted to; see later) reflections with  $h-k$   
46  $\neq 3N$  and  $l = 4M \pm 1$  (see Figs. 8a and 9a), as it is expected for layer-faulting induced line  
47 broadening for the C36 modification (cf. Table 2). The extent of the line broadening for  
48 these reflections increases with  $l$  (Fig. 9a), leading to almost complete undetectability of  
49 reflections of high  $l$  values (see e.g. the 105 and 107 reflections in Fig. 8a). All other  
50 reflections exhibit no appreciable broadening. Hence,  $(0,0,1/2)$  is the predominant  
51 displacement vector (cf. Table 2). This conclusion is supported by the observation that in  
52  
53  
54  
55  
56  
57  
58  
59  
60

1  
2  
3 particular the 106 reflection (belonging to the  $h-k \neq 3N$  and  $l = 4M \pm 2$  reflection class) is  
4 narrow, whereas it would have broadened by the occurrence of all types of displacement  
5 vectors, in particular as promoted by its high  $l$  value, except for the occurrence of  
6  $(0,0,1/2)$  as displacement vector (Table 2).  
7  
8  
9

### 10 11 12 **3.1.3 HRTEM**

13  
14 A total of 15 crystallites from the NbCr<sub>2</sub> powder obtained from the top part of the as-cast  
15 ingot was examined by HRTEM. The C36 structure was found in 13 crystallites; in two  
16 cases together with some regions exhibiting the C14 modification and in two other cases  
17 together with some regions exhibiting the C15 modification. Only one crystallite was  
18 fully of the C14 modification, and one other crystallite was fully of the C15 modification.  
19 In many crystallites, a high density of layer-stacking irregularities was found, in  
20 association with streaks along the (hexagonal)  $\langle 0001 \rangle$  direction in the selected area  
21 diffraction (SAD) patterns (Fig. 10).  
22  
23  
24  
25  
26  
27

28 Single faults (i.e. only one isolated “incorrect” *transition* between two layers  
29 (actually, two layer-sandwich units) with respect to the C36 layer-stacking sequence; cf.  
30 Fig. 3)) were generally not found in the hexagonal C36 crystallites: instead, combinations  
31 of successive faults were observed which led to the emergence of intergrowth-type  
32 irregularities within the dominant C36 modification (Figs. 10 a-c). Similarly,  
33 intergrowth-type irregularities were observed within the minor retained C14 modification  
34 as well (Fig. 10d).  
35  
36  
37  
38  
39  
40

41 With reference to Table 1, in case of the C36 modification (stacking sequence  
42 ...chch...), one or multiple *2H-type* (C14-type) sequences (with stacking sequence -hh-)  
43 are observed (Fig. 10a) and one or multiple *6H-type* sequences (with stacking sequence -  
44 cchch-; Figs. 10b,c).  
45  
46  
47

48 In case of the C14 modification (stacking sequence ...hh...), frequently one or  
49 multiple *4H-type* (C36-type) sequences (with stacking sequence -chch-) are found (Fig.  
50 10d). For distinction between the periodic Laves-phase crystal structure matrices and the  
51 local stacking irregularities, the Ramsdell notation is used for the stacking irregularities  
52 and the Strukturbericht designation for the matrices. Further, the periodic stacking  
53 sequences of the crystal structures will be enframed by the symbol “...”, whereas the  
54  
55  
56  
57  
58  
59  
60

1  
2  
3 local stacking irregularities will be enframed by the symbol “-“ to distinguish between  
4 the periodic stacking sequences of the matrices and the local layer configuration at the  
5 layer-stacking irregularities.  
6  
7  
8  
9

## 10 11 12 13 14 15 16 17 18 **3.2 TiCr<sub>2</sub>**

### 19 **3.2.1 Phase analysis and composition**

20 The as-cast and heat treated (cf. section 2.1) specimen consisted fully of C36-Laves  
21 phase (as determined by X-ray diffraction). According to wavelength dispersive X-ray  
22 analysis (WDX-EPMA) the composition of the Laves phase obeys (35.6 ± 0.3) at.% Ti  
23 and (64.4 ± 0.3) at.% Cr in agreement with the target composition (section 2.1).  
24  
25  
26  
27

28 By optical microscopy and SEM the presence of a minority phase was detected  
29 (volume fraction approx. 1 % as determined by area analysis). The phase was identified  
30 by EBSD as a bcc phase. Standardless EDX analysis revealed that the minority phase is a  
31 Ti-rich phase. In view of the Ti-Cr phase diagram this suggests that this phase is the β-Ti  
32 solid solution.  
33  
34  
35  
36  
37  
38  
39  
40

### 41 **3.2.2 XRPD**

42 The diffraction pattern of the coarse powder (cf. section 2.1) of the C36 phase is shown  
43 in Fig. 8b. The FWHM of the reflections (shown in Fig. 8b), after correction for  
44 instrumental broadening (see section 2.3), has been plotted as function of the diffraction  
45 vector  $Q$  in Fig. 9b.  
46  
47  
48

49 The 110 reflection belongs to the class of reflections with  $h - k = 3N$  and  $l = 4M$ .  
50 These reflections show no peak broadening due to layer-stacking irregularities (see Table  
51 2), so that only broadening due to finite crystallite size and due to microstrains, caused by  
52 defects or composition variations, is possibly exhibited by these reflections. Assuming  
53 that the whole broadening of the 110 reflection is due to microstrain-like broadening  
54  
55  
56  
57  
58  
59  
60

1  
2  
3  
4  
5  
6  
7  
8  
9  
10  
11  
12  
13  
14  
15  
caused by composition variations, an upper boundary for the width of the composition distribution equal to  $B_{\xi} = 0.56$  at.% was calculated from the FWHM of the 110 reflection according to the method given in Ref. [24]. This  $B_{\xi}$  is the FWHM of a super-Lorentzian ( $\eta = 1.2$ , see section 2.3) probability density function of the composition on the at.%-scale. Thus the maximum compositional variation was determined to be  $\pm 0.28$  at.%. This value is within the standard deviation of the WDX-EPMA analysis (cf section 3.2.1): such compositional variation cannot be exposed by WDX-EPMA analysis.

16  
17  
18  
19  
20  
21  
22  
23  
24  
25  
26  
27  
28  
29  
30  
31  
The peak broadening is affected by the grinding procedure: the peaks of the fine powder (more severely ground) are somewhat broader than the peaks of the coarse powder (less severely ground; see Fig. 9b). This includes the reflection class with  $h - k = 3N$  and  $l = 4M$ , as well. Since the  $h - k \neq 3N$  reflections (which should show peak broadening due to (also) the layer-stacking irregularities, in addition to microstrains, as discussed above (cf. Table 2)) of the fine powder, as compared to the coarse powder, reveal extra broadening to about the same extent as reflections of the reflection class with  $h - k = 3N$  and  $l = 4M$ , it can be concluded that the grinding procedure does not influence the layer-stacking irregularity density.

32  
33  
34  
35  
36  
37  
38  
39  
40  
41  
42  
43  
44  
45  
46  
47  
48  
49  
The powder-diffraction pattern of the C36 phase exhibits a distinctly  $hkl$ -dependent broadening of reflections, which is of the same type as observed for C36-NbCr<sub>2</sub> (see section 3.1.2): The reflections with  $h - k \neq 3N$  and  $l = 4M \pm 1$  show a considerable peak broadening. This means that in the case of TiCr<sub>2</sub> also (0,0,1/2) is the predominant displacement vector. However, in contrast to C36-NbCr<sub>2</sub>, the reflections with  $h - k \neq 3N$  and  $l = 4M$  (e.g. 204) and those with  $h - k \neq 3N$  and  $l = 4M + 2$  (e.g. 106) show a slightly larger peak broadening than the reflections with  $h - k = 3N$  and  $l = 4M$ . This indicates that in case of TiCr<sub>2</sub> also layer-stacking irregularities with displacement vectors different from (0,0,1/2) occur.

### 50 51 52 53 54 55 56 57 58 59 60 3.2.3 HRTEM

A total of eight crystallites were investigated by HRTEM. All crystallites are dominantly composed of the C36 modification. In one crystallite within the C36 phase a  $2H$ -type (C14-type) stacking irregularity was found and in another a  $6H$ -type stacking irregularity was found. Furthermore in one crystallite both an accumulation of three consecutive  $2H$ -

1  
2  
3  
4  
5  
6  
7  
8  
9  
10  
11  
12  
13  
14  
15  
16  
17  
18  
19  
20  
21  
22  
23  
24  
25  
26  
27  
28  
29  
30  
31  
32  
33  
34  
35  
36  
37  
38  
39  
40  
41  
42  
43  
44  
45  
46  
47  
48  
49  
50  
51  
52  
53  
54  
55  
56  
57  
58  
59  
60

*type* (-hh-) and a *6H-type* (-cchcch-) stacking irregularity was found (see Fig. 11a). In addition one crystallite contained a “split” *6H-type* stacking sequence (i.e. two -cch- stacking sequences separated by a larger C36 block; see Fig. 11b). In general, in the investigated C36-TiCr<sub>2</sub> specimens much fewer stacking irregularities occur than in the investigated C36-NbCr<sub>2</sub> specimens.

### 3.3 NbCo<sub>2</sub>

The line broadening visible in the XRPD data of C36-NbCo<sub>2</sub> differs distinctly from that observed for the NbCr<sub>2</sub> and TiCr<sub>2</sub> analogues (Figs. 8a,b vs. Fig. 8c). The reflections pertaining to all reflection classes with  $h - k \neq 3N$  experience considerable line broadening (Fig. 9c), in particular the prominent 106 reflection (belonging to the  $h - k \neq 3N$  and  $l = 4M + 2$  class of reflections) which is only marginally broadened in the case of the C36-TiCr<sub>2</sub> specimens (Fig. 9b) and not broadened at all for the C36-NbCr<sub>2</sub> specimens (Fig. 9a). Moreover, distinctly asymmetric diffraction-line broadening occurs for the  $h - k \neq 3N$  and  $l = 4M + 1$  class of reflections, which has been reported in Ref. [18] as representative for stacking-layer faulting not characterized by the (0,0,1/2) displacement vector.

## 4. Discussion

### 4.1 Stacking irregularities and associated displacement vectors

Two predominant types of stacking irregularities are found in the equilibrated C36-TiCr<sub>2</sub> specimen and in the as-cast C36-NbCr<sub>2</sub> specimen by HRTEM: *single* and/or *multiple 2H-type* and *6H-type* (intergrowth-type) stacking irregularities. Insertion of a *2H-type* irregularity in a perfect C36 (4H) crystal leads to a displacement vector of (0,0,1/2) (cf. section 1.2); insertion of a *6H type* irregularity requires a displacement vector of (0,0,3/2), which is equivalent to the displacement vector (0,0,1/2) due to the translational symmetry of the C36 (4H) crystal structure, comprising four layer-sandwich units (cf. Table 1). Further, because of this translational symmetry, accumulations of multiple *2H-type* or *6H-type* stacking irregularities, as frequently observed in the HRTEM images (e.g. Figs. 10c, 11a), can only add up to a displacement vector equivalent to (0,0,0), which causes no peak broadening, or (0,0, 1/2) which leads to broadening of reflections

of the class with  $h - k \neq 3N$  and  $l = 4M \pm 1$ . Then also reflections of the class with  $h - k \neq 3N$  and  $l = 4M + 2$  remain narrow, which would be not the case for (all) other possible displacement vectors (cf. Table 2).

Exactly these above-indicated broadening characteristics are observed in the XRPD patterns of C36-NbCr<sub>2</sub> and in those of C36-TiCr<sub>2</sub> (where the broadening was less pronounced).

A special case is the “split” *6H*-type irregularity observed in TiCr<sub>2</sub> (cf. Fig. 11b). The displacement between the middle 4H (C36) part, which is bounded by the two -cch-stacking irregularities, which can be regarded as a split-up 6H (-cchcch-) stacking sequence, and the two adjacent parts of the 4H crystal is of type  $\pm(1/3, 2/3, +1/4)$ ; the displacement vector between the two adjacent parts of the 4H crystal separated by the whole “split” *6H*-type irregularity is again of type  $(0,0,1/2)$ .

HRTEM and XRPD line-profile analysis give complementary results: HRTEM reveals the detailed structure of individual stacking irregularities, whereas XRPD provides data pertaining to the average microstructure. It thus follows that the *2H*-type and *6H*-type stacking irregularities are the dominating layer-stacking defects in C36-type NbCr<sub>2</sub> and TiCr<sub>2</sub> Laves phases.

## 4.2 Relation with phase-transformation mechanism

### 4.2.1 General remarks

The similarity of the stacking irregularities occurring in C36-TiCr<sub>2</sub> and C36-NbCr<sub>2</sub> (i.e. the occurrence of the same type of displacement vector; cf. section 4.1) suggests that the origin of these stacking irregularities is the same for both Laves phases. A very remarkable feature of the stacking irregularities with a displacement vector of  $(0,0,1/2)$ , is that no shear displacement of the part of the crystal above the irregularity occurs with respect to the part of the crystal below the irregularity: i.e.  $u' = v' = 0$  (see Fig. 7). It can thus be concluded that these stacking irregularities are not induced by plastic deformation processes possibly occurring during sample preparation, e.g. by thermal stresses. Indeed, as demonstrated in section 3.1.3, the grinding procedure has no influence on the density of the stacking irregularities.

1  
2  
3  
4  
5  
6  
7  
8  
9  
10  
11  
12  
13  
14  
15  
16  
17  
18  
19  
20  
21  
22  
23  
24  
25  
26  
27  
28  
29  
30  
31  
32  
33  
34  
35  
36  
37  
38  
39  
40  
41  
42  
43  
44  
45  
46  
47  
48  
49  
50  
51  
52  
53  
54  
55  
56  
57  
58  
59  
60

It is supposed that both C36 Laves phases, NbCr<sub>2</sub> and TiCr<sub>2</sub>, have been formed from a C14-type structure, which evolves in case of NbCr<sub>2</sub> as a metastable state (cf. section 3.1.1) during solidification at certain locations in the ingot [19, 23] and in case of TiCr<sub>2</sub> as a stable state during the decrease of annealing temperature from 1395°C (bcc-solid solution) to 1200°C (cf. phase diagram, Fig. 6b); in this temperature range, the C14 phase field of TiCr<sub>2</sub> is passed. In section 1.2 it has been discussed how a C14 crystal can transform into C36 by passage of a periodic series of synchro-Shockley partial dislocation dipoles (“ordered glide”, Figs. 4, 5). The passage of one synchro-Shockley partial dislocation dipole within a C14 structure (as shown in Fig. 4), generates a layer-stacking irregularity of 4H-type (C36-type) –YZYX- (-chch-) into the ...XYXY... (...hh...) stacking sequence of C14. Due to the opposite sign of the Burgers vectors of the partial dislocations forming the dipole, the overall Burgers vector associated with this defect is zero, and thus no macroscopic displacement will be induced between the parts of the C14 crystal adjacent to such a defect (see Fig. 4). Such 4H-type layer stacking irregularities are experimentally observed in the retained NbCr<sub>2</sub>-C14 crystallites (Fig. 10d). Only “ordered glide”, i.e. glide of a synchro-Shockley partial dislocation dipole on (i.e. above and below) every fourth layer-sandwich unit over a certain range of the C14 crystal, generates the C36 modification. This “ordered glide” requires coordination of the gliding partial-dislocation dipoles in order to produce C36. If this order is kept perfectly over the whole crystal, a defect-free, perfect C36 crystal would result, and hence no layer-stacking irregularities (with respect to the C36 layer stacking) and no corresponding reflection broadening would occur.

Irregularities in the passage of the synchro-Shockley partial dislocation dipoles (i.e. deviations from “ordered glide”) can be the origin of the layer-stacking irregularities in the C36-Laves phases as observed by HRTEM and XRPD in this work. Two mechanisms, which can occur simultaneously, are proposed in the following to explain the observed deviations. The first mechanism (section 4.2.2) derives from the recognition that four different but energetically equivalent modes for formation of C36 are possible, depending on which of the four possible layers within two consecutive C14 unit cells (i.e. XYXY) is shifted to produce C36 (cf. Fig. 4). If more than one of these modes is operative within one parent C14 crystal, initiating from different locations within the

1  
2  
3  
4  
5  
6  
7  
8  
9  
10  
11  
12  
13  
14  
15  
16  
17  
18  
19  
20  
21  
22  
23  
24  
25  
26  
27  
28  
29  
30  
31  
32  
33  
34  
35  
36  
37  
38  
39  
40  
41  
42  
43  
44  
45  
46  
47  
48  
49  
50  
51  
52  
53  
54  
55  
56  
57  
58  
59  
60

crystal, different C36 *domains* form, and layer-stacking irregularities occur upon impingement of these domains (Fig. 12). Yet, this first mechanism involves perfect, “ordered glide” within each domain. The second mechanism (section 4.2.3) involves the occurrence of local deviation from “ordered glide”, i.e. within a domain, leading to breaking up of the domain into *regimes*.

#### 4.2.2 Domain formation

The requirement that every fourth layer-sandwich unit has to be displaced for the formation of C36 from C14 necessitates to distinguish between every two adjacent layer-sandwich units in C14, which is done here by introducing Roman numerals as subscript (see Fig. 13); the stacking sequence of a C14 crystallite would thus be ...X<sub>I</sub>Y<sub>I</sub>X<sub>II</sub>Y<sub>II</sub>.... A C36 stacking can then be formed by shifting either all X<sub>I</sub> to Z or all X<sub>II</sub> to Z or all Y<sub>I</sub> to Z or all Y<sub>II</sub> to Z (cf. also Fig. 13). Taking the initial C14 structure as reference, four different C36 product domains can thus be formed (similar to the domains found e.g. in ordered substitutional intermetallics/phases). In the first two cases, the shift is realized by a dipole consisting of the synchro-Shockley partial-dislocation pair  $\mathbf{b}_i/-\mathbf{b}_i$ , while in the last two cases, the pair of synchro-Shockley partial dislocations is  $-\mathbf{b}_i/\mathbf{b}_i$  (cf. Fig. 2) Note that the first Burgers vector of the pair indicates the shift of the layer-sandwich unit with respect to the, say, bottom part of the crystal concerned, while the second Burgers vector is necessary to shift (reversely) the, say, top part of the crystal back to its original position, thereby avoiding macroscopic shear of the crystal (see Fig. 4). The four possible C36 structures formed by the four layer-shift options are not identical, but displaced with respect to each other by the displacement vectors indicated in Fig.13 and provided by Table 3<sup>3</sup>. The C36 domains thus formed either grow in *c* (stacking) direction by “ordered glide” of more synchro-Shockley partial-dislocation dipoles shifting the same type of layer-sandwich unit, or new domains form between the existing ones, which is shown schematically in Fig. 12. Growth of existing domains and formation of new domains may also occur simultaneously. The crystal can be regarded as completely transformed from C14 to C36 after impingement of these domains.

---

<sup>3</sup> The layer-stacking irregularity occurring between a pair of such domains can be conceived as an anti-phase boundary.

1  
2  
3  
4  
5  
6  
7  
8  
9  
10  
11  
12  
13  
14  
15  
16  
17  
18  
19  
20  
21  
22  
23  
24  
25  
26  
27  
28  
29  
30  
31  
32  
33  
34  
35  
36  
37  
38  
39  
40  
41  
42  
43  
44  
45  
46  
47  
48  
49  
50  
51  
52  
53  
54  
55  
56  
57  
58  
59  
60

A perfect (i.e. stacking-fault or layer-stacking irregularity free) C36 crystal can only result from a parent C14 crystal if *only one* of the above four layer-sandwich unit shift options is adopted throughout the crystal. In this case, for transitional stages as well as for the end stage of the transformation, the displacement vectors between the various C36 domains would always be (0,0,0), and thus no phase shift of diffracted waves and hence no reflection broadening of reflections originating from the C36 domains in the XRPD pattern can occur. In this case, after impingement of the growing domains, a perfect C36 stacking sequence over the whole initial C14 crystallite results.

If the four types of domains shown in Fig. 13 would occur randomly within a parent C14 crystal, the impingement (of the domains growing in the *c*-direction) between different domains, will lead to “anti-phase boundaries” (see footnote 3) because of the displacement between two impinging C36 structures: stacking irregularities occur associated with corresponding broadening of XRPD reflections according to the theoretical considerations in section 1.3. Two types of displacement vectors can be indicated:  $(1/3, 2/3, 1/4)$  and  $(0, 0, 1/2)$ , with the first ones occurring statistically twice as frequently as the latter one if all four types of domains occur randomly (see Fig. 13). This last phenomenon is not compatible with the present observations for the C36-NbCr<sub>2</sub> and C36-TiCr<sub>2</sub> specimens, revealing a predominant broadening of the reflections of the class with  $h - k \neq 3N$  and  $l = 4M \pm 1$ , which implies that the  $(0, 0, 1/2)$  displacement vector is dominant, i.e. only X or only Y layer-sandwich units have been displaced within a parent C14 crystal (cf. Fig. 13). In the case of TiCr<sub>2</sub>, also  $h - k \neq 3N$  reflections not pertaining to  $l = 4M \pm 1$  are slightly broadened suggesting a minor mixed occurrence (i.e. both X and Y) of layer-sandwich unit displacements within a parent C14 crystal. The “split” *6H-type* irregularity (Fig. 11b; see section 3.2.3) can thus be conceived as the outcome of impingement of three C36 domains. The upper and lower one are formed by e.g. shifts of X layers (e.g. X<sub>I</sub> in the lower and X<sub>II</sub> in the upper domain), whereas the middle domain is formed by e.g. shifting Y<sub>II</sub> layers.

Table 3: Displacement vectors between C36 domains, produced in a parent C14 crystal by the synchro-Shockley partial dislocation dipole mechanism, by shifting for each

domain one of the four different layer-sandwich units of the ...X<sub>I</sub>Y<sub>I</sub>X<sub>II</sub>Y<sub>II</sub>... sequence in the parent C14 structure to Z position (see Fig. 13).

	X <sub>I</sub> to Z	X <sub>II</sub> to Z	Y <sub>I</sub> to Z	Y <sub>II</sub> to Z
X <sub>I</sub> to Z	(0,0,0)	(0,0,1/2)	(1/3,2/3,1/4)	(1/3,2/3,1/4)
X <sub>II</sub> to Z	(0,0,1/2)	(0,0,0)	(1/3,2/3,1/4)	(1/3,2/3,1/4)
Y <sub>I</sub> to Z	(1/3,2/3,1/4)	(1/3,2/3,1/4)	(0,0,0)	(0,0,1/2)
Y <sub>II</sub> to Z	(1/3,2/3,1/4)	(1/3,2/3,1/4)	(0,0,1/2)	(0,0,0)

### 4.2.3 Transformation errors

The “ordered glide” of synchro-Shockley partial dislocation dipoles is induced and controlled by the associated decrease in Gibbs energy of the transforming Laves phase (cf. section 4.2.1). The “ordered glide” and thus the stacking sequence of the resulting C36 crystal will be practically perfect, if the energy “penalty” for deviations from this perfectly ordered glide is high compared to the decrease of Gibbs energy achieved by the transformation from C14 to C36. In case of Laves phases, the Gibbs energies of the different layer-sandwich unit stacking modifications differ only slightly (e.g. [25]) and hence the stacking fault energy is also low. Thus, deviations from perfect “ordered glide” are likely.

Irrespective of the precise origin of deviations from perfect “ordered glide”, the most likely deviations are those which correspond most closely to the state of perfect order. Such most likely deviations are those which, nevertheless, satisfy the following characteristics of the *perfect* phase transformation:

- Glide of only synchro-Shockley partial dislocation *dipoles* is required to realize the irregularity
- Within one transforming domain, either only X or only Y layers are shifted to Z.

The last point involves that glide is realized by either only dipoles with the Burgers vectors  $\mathbf{b}_i/\mathbf{b}_i$  or only dipoles with the Burgers vectors  $-\mathbf{b}_i/\mathbf{b}_i$ .

Under these constraints, disorder in the passage of synchro-Shockley partial dislocation dipoles during the transformation occurs by a change of either X<sub>I</sub> to X<sub>II</sub> or Y<sub>I</sub>

1  
2  
3 to  $Y_{II}$  for the shifting layer-sandwich unit (Fig. 14). Such changes can occur if either of  
4  
5 the following scenarios takes place:

- 6  
7 (i) One (say, either  $X_I$  or  $Y_I$ ) layer, which should have shifted according to  
8 perfect “ordered glide”, remains immobile and “ordered glide”, supposed to  
9 proceed in the  $c$ -direction, is continued by shifting the other representatives of  
10 the layers of the same stacking position (i.e. either  $X_{II}$  or  $Y_{II}$ , Fig. 14a)  
11  
12 (ii) A change of shifting layer (from either  $X_I$  to  $X_{II}$  or  $Y_I$  to  $Y_{II}$ ) occurs without  
13 such preceding immobilisation, i.e. the distance between two shifted layers is  
14 two instead of four layers (Fig. 14b).  
15  
16  
17  
18

19 Both such local deviations from perfect “ordered glide” are accompanied by the  
20 introduction of 2H-type layer-stacking irregularities; the displacement vector between the  
21 different 4H (C36) regimes is  $(0,0,1/2)$ .  
22  
23

24 Another possibility to introduce stacking irregularities in the product C36 crystal  
25 is that some of the synchro-Shockley partial dislocation dipoles are not separated by only  
26 one (cf. Fig. 4) but by three layer-sandwich units (see Fig. 15a). Such deviations also  
27 bring about a change of shifted layer type from either  $X_I$  to  $X_{II}$  or  $Y_I$  to  $Y_{II}$ , or vice-versa.  
28 The local stacking irregularity formed by such an “expanded” dipole is of  $6H$  type, the  
29 corresponding displacement vector between the adjacent 4H (C36) regimes is  $(0,0,1/2)$ .  
30  
31  
32  
33  
34

35 Formation of  $6H$ -type layer-stacking irregularities (Fig. 15) may be a way to  
36 lower the energy increase associated with the introduction of the  $2H$ -type layer-stacking  
37 irregularities described above (Fig. 14). This could occur upon further cooling (i.e. after  
38 completion of the  $C14 \rightarrow C36$  transformation, assuming that (for some temperatures  
39 range) below the  $C14 \rightarrow C36$  transformation temperature, a 6H stacking sequence has a  
40 lower Gibbs energy than a 2H stacking sequence. This process is shown in Fig. 15b. It  
41 requires (with respect to Burgers vector pair) passage of the type of synchro-Shockley  
42 partial dislocation dipole with Burgers vectors of opposite signs as compared to those  
43 operating upon formation of the C36 structure from the parent C14 structure.  
44  
45  
46  
47  
48  
49  
50  
51

### 52 53 **4.2.3 Overall discussion**

54 In the two preceding sections, two mechanisms have been presented which induce  
55 stacking irregularities into a C36 product structure formed from a C14 parent structure by  
56  
57  
58  
59  
60

1  
2  
3 otherwise perfect “ordered glide” of synchro-Shockley partial dislocation dipoles.  
4 According to the first mechanism (section 4.2.1) four different types of domains can be  
5 formed, which are not “in phase” with respect to each other, causing layer-stacking  
6 irregularities upon impingement of the domains. Within each domain perfect “ordered  
7 glide” of synchro-Shockley partial dislocation dipoles takes place and thus no layer-  
8 stacking irregularities occur within the domains. Two different displacement vectors  
9 occur between the different domains in this model:  $(1/3, 2/3, 1/4)$  and  $(0, 0, 1/2)$ . In case of  
10 random occurrence of all four domain types the first displacement vector  $(1/3, 2/3, 1/4)$   
11 occurs statistically twice as often as the displacement vector  $(0, 0, 1/2)$ . The  
12 experimentally observed dominance of the  $(0, 0, 1/2)$  displacement vector thus is ascribed  
13 to the presence of  $2H$ - and  $6H$ -type irregularities, induced by the second mechanism to  
14 generate stacking irregularities, i.e. by deviations from perfect “ordered glide” of  
15 synchro-Shockley partial dislocation dipoles during the transformation in a single domain  
16 (section 4.2.2), leading to regime formation within the domains. It is shown that the  
17 smallest possible and simplest deviations lead to the  $2H$ - and  $6H$ -type layer-stacking  
18 irregularities as observed by HRTEM, associated with a displacement vector between the  
19 adjacent C36 crystal regimes of  $(0, 0, 1/2)$ , as deduced from XRPD-line profile analysis.  
20  
21  
22  
23  
24  
25  
26  
27  
28  
29  
30  
31  
32

33 The two mechanisms for generating stacking irregularities can operate jointly.  
34 Domain formation and impingement can occur *together* with flawed “ordered glide”  
35 during the transformation *within* the forming domains (transformation errors). The case  
36 that regime boundaries occur more frequently than domain boundaries has been  
37 schematically illustrated in Fig. 16. In this case, using HRTEM, the probability of finding  
38 a  $2H$ -type or  $6H$ -type layer-stacking irregularity would be much higher than finding a  
39 domain boundary. Also the line broadening in XRPD patterns originating from such C36  
40 structures would be dominated by the displacement vector  $(0, 0, 1/2)$ , inducing pronounced  
41 broadening of reflections of the class with  $h-k \neq 3N$  and  $l = 4M \pm 1$ . These predictions  
42 regarding the HRTEM and XRPD data agree fully with the corresponding observations  
43 made on C36-NbCr<sub>2</sub>. Domain boundaries associated with a displacement vector of  
44  $(1/3, 2/3, 1/4)$  would also induce some minor broadening of reflections of the classes  $h-k \neq$   
45  $3N$  with  $l = 4M$  and  $h-k \neq 3N$  with  $l = 4M + 2$ , in addition to broadening of reflections of  
46  
47  
48  
49  
50  
51  
52  
53  
54  
55  
56  
57  
58  
59  
60

1  
2  
3 the class  $h-k \neq 3N$  and  $l = 4M \pm 1$ . This is in agreement with the experimental  
4 observations made on C36-TiCr<sub>2</sub>.  
5  
6

7 The C36-NbCo<sub>2</sub> structure does not form by a C14 → C36 transformation. Although  
8 a C14-NbCo<sub>2</sub> Laves phase exists at high Nb content, it is separated from the C36-phase  
9 field in the Nb-Co phase diagram by a C15-NbCo<sub>2</sub> phase [16] (see Fig. 6c). Thus, the  
10 preferential formation of stacking irregularities with a (0,0,1/2) displacement vector,  
11 based on formation of C36 from (fault-free) C14, cannot pertain to C36-NbCo<sub>2</sub>. The  
12 discussion of possible origins for the stacking-layer irregularities in C36-NbCo<sub>2</sub>  
13 (associated with only a minor occurrence of the displacement vector (0,0,1/2), but with  
14 major occurrence of other displacement vectors as listed in Table 2; see results reported  
15 in section 3.1) is beyond the scope of the present paper.  
16  
17  
18  
19  
20  
21  
22  
23  
24

## 25 5. Conclusions

- 26  
27 i. Irregularities in the layer-sandwich unit stacking sequences of C36 Laves phases  
28 (TiCr<sub>2</sub> and NbCr<sub>2</sub>), which form from C14-type precursors, have been exhibited by  
29 HRTEM and XRPD-line profile analysis. The occurrence of such faulting  
30 provides validation of the proposed mechanism for the C14 → C36 phase  
31 transformation by glide of a series of ordered synchro-Shockley partial dislocation  
32 dipoles (“ordered glide”).  
33  
34  
35  
36  
37 ii. Two mechanisms bringing about the (layer-sandwich unit) stacking irregularities  
38 have been identified:  
39  
40 • Domain formation: Four different types of perfect C36 domains, which are  
41 displaced with respect to each other, occur simultaneously within one parent C14  
42 crystal, leading to layer-stacking irregularities upon impingement of the growing  
43 domains.  
44  
45 • Transformation errors: Deviations occur from perfect “ordered glide” during the  
46 transformation within a domain.  
47  
48  
49  
50  
51 iii. The predominant layer-stacking irregularities are *2H*- and *6H*-type stacking  
52 sequences within a domain, as evidenced by HRTEM and XRPD (selective  
53 broadening of the class of XRPD reflections with  $h - k \neq 3N$  and  $l = 4M \pm 1$   
54 implying that stacking faults with a displacement vector of (0,0,1/2) are  
55  
56  
57  
58  
59  
60

1  
2  
3 dominant): The transformation errors are the dominating layer-sandwich unit  
4 stacking irregularities for the investigated C36-NbCr<sub>2</sub> and C36-TiCr<sub>2</sub> Laves  
5 phases. The contribution of domain boundaries is negligible compared to that of  
6 the regime boundaries in case of C36-NbCr<sub>2</sub>, but less so in case of C36-TiCr<sub>2</sub>.  
7  
8

- 9  
10  
11 iv. C36-NbCo<sub>2</sub>, which is not formed from a C14 precursor, (indeed) shows faulting  
12 distinctly different from C36-TiCr<sub>2</sub> and C36-NbCr<sub>2</sub>.  
13

## 14 15 16 **6. Acknowledgement**

17 The authors are grateful to Mr. Thomas Meisner (Max Planck Institute for Metals  
18 Research) for indispensable collaboration during alloy preparation. The diffraction pattern  
19 of NbCo<sub>2</sub> was kindly provided by Dr. Daniel Grüner and Dr. Guido Kreiner (Max Planck  
20 Institute for Chemical Physics of Solids, Dresden, Germany). The authors also thank  
21 Prof. Dr. Arndt Simon (Max Planck Institute for Metals Research, Stuttgart) for use of his  
22 TEM facilities. This work has been performed within the framework of the Inter-  
23 Institutional Research Initiative "The Nature of Laves Phases" funded by the Max Planck  
24 Society.  
25  
26  
27  
28  
29  
30  
31  
32

## 33 34 **7. Literature**

- 35 [1] Sauthoff, G. (1995). "Intermetallics". Weinheim, VCH.  
36  
37 [2] Stein, F., Palm, M. and Sauthoff, G. (2004). *Intermetallics* 12: 713-720.  
38  
39 [3] Stein, F., Palm, M. and Sauthoff, G. (2005). *Intermetallics* 13: 1056-1074.  
40  
41 [4] Frank, F. C. and Kasper, J. S. (1958). *Acta Crystallographica* 11(3): 184-190.  
42  
43 [5] Frank, F. C. and Kasper, J. S. (1959). *Acta Crystallographica* 12(7): 483-499.  
44  
45 [6] Allen, C. W., Delavignette, P. and Amelinckx, S. (1972). *Phys. Status Solidi A* 9:  
46 237.  
47  
48 [7] Hazzledine, P. M. and Pirouz, P. (1993). *Scr. Metall. Mater.* 28: 1277-1282.  
49  
50 [8] Kumar, K. S. and Hazzledine, P. M. (2004). *Intermetallics* 12: 763-770.  
51  
52 [9] Jagodzinski, H. (1949). *Acta Crystallogr., Sect. A: Found. Crystallogr.* 2: 201-  
53 207.  
54  
55  
56  
57  
58  
59  
60

- 1  
2  
3  
4  
5 [10] Ramsdell, L. S. (1947). *Am. Mineral.* 32(1-2): 64-82.  
6  
7 [11] Barrett, M. A. and Massalski, T. B. (1966). "The structure of metals", McGraw-  
8 Hill, New York.  
9  
10 [12] Allen, C. W. and Liao, K. C. (1979). *Proceedings of the ICOMAT Boston 1979*:  
11 124-129.  
12  
13 [13] Liao, K. C. and Allen, C. W. (1981). *Proceedings of the International Conference*  
14 *of Solid-Solid Phase Transformations*: 1493-1497.  
15  
16 [14] Allen, C. W. and Liao, K. C. (1982). *Phys. Status Solidi A* 74: 673-681.  
17  
18 [15] Chisholm, M. F., Kumar, S. and Hazzledine, P. (2005). *Science* 307: 701-703.  
19  
20 [16] Leoni, M. (2008). *Z. Kristallogr.* 223(9): 561-568.  
21  
22 [17] Prasad, B. and Lele, S. (1971). *Acta Crystallogr., Sect. A: Found. Crystallogr.* 27:  
23 54-64.  
24  
25 [18] Michalski, E., Kaczmarek, S. and Demianiuk, M. (1988). *Acta Crystallogr., Sect.*  
26 *A: Found. Crystallogr.* 44: 650-657.  
27  
28 [19] Aufrecht, J., Leineweber, A. and Mittemeijer, E. J. (2008). *Mater. Res. Soc. Symp.*  
29 *Proc.* 1128: 481-486.  
30  
31 [20] Gruener, D., Stein, F., Palm, M., Konrad, J., Ormeci, A., Schelle, W., Grin, Y.  
32 and Kreiner, G. (2006). *Z. Kristallogr.* 221(5-7): 319-333.  
33  
34 [21] La Pouchau, J. L. and Pichoir, F. (1984). *Recherche Aerospatiale* 3: 167-192.  
35  
36 [22] (2003). Topas, General Profile and Structure Analysis Software for Powder  
37 Diffraction Data, Version 3, Bruker AXS GmbH, Karlsruhe.  
38  
39 [23] Aufrecht, J., Leineweber, A., Senyshyn, A. and Mittemeijer, E. J. (2010). *Scripta*  
40 *Materialia* 62(5): 227-230.  
41  
42 [24] Leineweber, A. and Mittemeijer, E. J. (2004). *J. Appl. Crystallogr.* 37: 123-135.  
43  
44 [25] Vedmedenko, O., Rösch, F. and Elsässer, C. (2008). *Acta Mater.* 56, 4984-4992.  
45  
46 [26] Thoma, D. J. and Perepezko, J. H. (1992). *Mater. Sci. Eng., A* 156: 97-108.  
47  
48 [27] Zhuang, Z., Shen, J., Liu, Y., Ling, L., Shang, S., Du, Y. and Schuster, J. C.  
49 (2000). *Z. Metallkd.* 91: 121.  
50  
51  
52  
53  
54  
55  
56  
57  
58  
59  
60

- 1  
2  
3  
4 [28] Okamoto, H. (2002). *Journal of Phase Equilibria* 23(382).  
5  
6  
7 [29] Stein, F., Jiang, D., Palm, M., Sauthoff, G., Grüner, D. and Kreiner, G. (2008).  
8 *Intermetallics* 16: 785-792.  
9  
10  
11  
12  
13  
14  
15  
16  
17  
18  
19  
20  
21  
22  
23  
24  
25  
26  
27  
28  
29  
30  
31  
32  
33  
34  
35  
36  
37  
38  
39  
40  
41  
42  
43  
44  
45  
46  
47  
48  
49  
50  
51  
52  
53  
54  
55  
56  
57  
58  
59  
60

For Peer Review Only

### Figure captions

Fig. 1: Schematic crystal structure of (a) C14 type Laves phase and (b) C36 type Laves phase, built up by alternate stacking of  $AB_3A$  *layer-sandwich units* and  $B$  *single-layer units*. In the upper part of the figure, the layer-stacking sequences have been displayed in a  $[11\bar{2}0]$  projection, i.e. the  $[11\bar{2}0]$  direction is perpendicular to the plane of drawing. In the lower part of the figure, the stacking positions have been indicated in  $[0001]$  projection. The basis vectors  $\mathbf{a}$  and  $\mathbf{b}$ , perpendicular to the stacking  $[0001]$  direction, span a two-dimensional hexagonal unit mesh.

Fig. 2: Stacking positions and Burgers vectors of partial dislocations in a  $(0001)$  plane of a Laves phase.

Fig. 3: Change of layer-stacking sequence by glide of a single synchro-Shockley partial dislocation. The *layer-sandwich unit*  $AB_3A$ , denoted by X in the left part of the figure, and the *single-layer unit*  $B$ , denoted by z in the left part of the figure, are shifted along the  $(0001)$  glide plane according to different Burgers vectors, as indicated in the  $[0001]$  projection in the bottom part of the figure: the white arrows correspond to the Burgers vector associated with the shift of the *layer-sandwich unit*; the black arrows correspond to the Burgers vector associated with the shift of the *single-layer unit*. The symbols  $\overline{\perp}$  and  $\perp$  denote single synchro-Shockley partial dislocations with Burgers vectors of opposite sign. The symbols  $\perp$  or  $\overline{\perp}$  do *not* specify whether the dislocation is of edge-, screw- or mixed character.

Fig. 4: Change of stacking sequence in a Laves-phase crystal (as indicated by the layer-sandwich units) by passage of a synchro-Shockley partial dislocation *dipole*, in order to preserve the external shape of the crystal: note the absence of *macroscopic* shear for the crystal concerned, in contrast with the situation realized by passage of a single synchro-Shockley partial dislocation as sketched in Fig. 3. For white and black arrows, see Fig. 3. The grey arrow indicates the effective shift of the middle layer-sandwich upon passage of the dipole.

1  
2  
3  
4  
5  
6  
7  
8  
9  
10  
11  
12  
13  
14  
15  
16  
17  
18  
19  
20  
21  
22  
23  
24  
25  
26  
27  
28  
29  
30  
31  
32  
33  
34  
35  
36  
37  
38  
39  
40  
41  
42  
43  
44  
45  
46  
47  
48  
49  
50  
51  
52  
53  
54  
55  
56  
57  
58  
59  
60

Fig. 5: Formation of the 4H stacking sequence of C36 from the 2H stacking sequence of C14 by passage by glide of an ordered sequence of synchro-Shockley partial dislocation dipoles (the symbols  $\overline{\text{—}}$  and  $\underline{\text{—}}$  denote single synchro-Shockley partial dislocations with Burgers vectors of opposite sign).

Fig. 6: Laves-phase containing composition ranges of the phase diagrams of the systems (a) Nb-Cr [26], (b) Ti-Cr [27, 28] and (c) Nb-Co [29]. Note that in case of NbCr<sub>2</sub> the C14-NbCr<sub>2</sub> Laves phase (and also the C36-NbCr<sub>2</sub> Laves phase) is no equilibrium phase, as shown recently in Ref. [23].

Fig. 7: Graphical illustration of the five different stacking-fault displacement vectors between two halves of a C36 crystal separated by a stacking irregularity. The actual, here arbitrarily chosen atomistic structure of the irregularity itself has no or negligible influence on the line broadening in reciprocal space. Because of the periodicity of the crystal structure, the two displacement vectors  $+(0, 0, 1/2)$  and  $-(0, 0, 1/2)$  are identical, whereas displacements as  $+(0, 0, 1/4)$  and  $-(0, 0, 1/4)$  are not identical but equivalent with respect to the resulting line broadening.

Fig. 8: X-ray powder diffraction patterns: (a) C36-NbCr<sub>2</sub>, powder as obtained from top of the arc-melted, solidified ingot (Cu-K $\alpha_1$  radiation); (b) C36-TiCr<sub>2</sub> produced by solid-state annealing for 50 h at 1200°C (coarse powder; Cu-K $\alpha_1$  radiation); (c) C36-NbCo<sub>2</sub> (Co-K $\alpha_1$  radiation). The Laue indices have been indicated.

Fig. 9: FWHM values of the reflections in the XRPD patterns of (a) C36-NbCr<sub>2</sub> as obtained from top of the arc-melted, solidified ingot (Cu-K $\alpha_1$  radiation), (b) C36-TiCr<sub>2</sub> produced by solid-state annealing for 50 h at 1200°C (coarse powder and fine powder, Cu-K $\alpha_1$  radiation) and (c) C36-NbCo<sub>2</sub> (Co-K $\alpha_1$  radiation).

Fig. 10: HRTEM images (C36 zone axis:  $\langle 11\bar{2}0 \rangle$ ) of material taken from the top of an as-cast NbCr<sub>2</sub> specimen: (a-c) C36 crystallites with (a) 2H-type stacking irregularities; single (b) or an accumulation of (c) 6H-type stacking irregularities and (d) a retained C14

1  
2  
3  
4  
5  
6  
7  
8  
9  
10  
11  
12  
13  
14  
15  
16  
17  
18  
19  
20  
21  
22  
23  
24  
25  
26  
27  
28  
29  
30  
31  
32  
33  
34  
35  
36  
37  
38  
39  
40  
41  
42  
43  
44  
45  
46  
47  
48  
49  
50  
51  
52  
53  
54  
55  
56  
57  
58  
59  
60

crystallite exhibiting *4H-type* stacking irregularities; (e) enlargement of a part of the SAD pattern shown as insert in (b), revealing the streaking along the (hexagonal)  $\langle 0001 \rangle$  direction. The arrows indicate the  $\langle 0001 \rangle$  direction.

Fig. 11: HRTEM images (C36 zone axis:  $\langle 11\bar{2}0 \rangle$ ) of annealed C36-TiCr<sub>2</sub> specimens containing stacking irregularities. (a) A *2H-type* (C14-type) and a *6H-type* stacking irregularity, (b) a “split” *6H-type* stacking irregularity. The arrows indicate the  $\langle 0001 \rangle$  direction.

Fig. 12: Formation of a C36 crystal by formation, growth and impingement of C36 domains

Fig. 13: The four different C36 domains which can evolve from the same C14 crystal by shifting layer-sandwich units and the single (B atom) layer in-between by the ordered passage (glide) of synchro-Shockley partial dislocation dipoles (see Figs. 4 and 5). The difference in Burgers vectors for the dipole pairs ( $\mathbf{b}_i/\mathbf{-b}_i$  if X is shifted to Z and  $\mathbf{-b}_i/\mathbf{b}_i$  if Y is shifted to Z) has been indicated by using the symbols  $\frac{\perp}{\bar{\perp}}$ , and  $\frac{\bar{\perp}}{\perp}$ . The corresponding displacement vectors between the resulting C36 domains have been indicated too. Note that for random occurrence of all four types of displacements (i.e. all four types of domains), the vector  $(1/3, 2/3, 1/4)$  occurs twice as frequently as the vector  $(0, 0, 1/2)$ . The latter displacement occurs exclusively, if within a transformed crystal, only X layers or only Y layers have been displaced, i.e. either only the two domains shown on the left or only the two domains shown on the right, occur.

Fig. 14: Possible deviations from perfect “ordered glide” of synchro-Shockley partial dislocation dipoles during a C14  $\rightarrow$  C36 transformation, subject to the constraint that only one type of synchro-Shockley partial dislocation dipoles is involved in the phase transformations, i.e. either only X or only Y layers are shifted to Z positions (cf. Fig. 13). For both cases shown in the figure, the layer shift switches from X<sub>I</sub> to X<sub>II</sub>. Contrarily to the occurrence of perfect “ordered glide” in the parent C14 crystal, where every second X

1  
2  
3 layer is shifted to Z, either one X layer to be shifted becomes immobilized (a), or two  
4 adjacent X layers (i.e. an  $X_I$  layer *and* an  $X_{II}$  layer) are shifted to Z (b). In both cases, a  
5  $2H$ -type stacking irregularity occurs.  
6  
7  
8  
9

10 Fig. 15: Formation of  $6H$ -type stacking irregularities (a) during or (b) subsequent to a  
11  $C14 \rightarrow C36$  phase transformation: (a) glide of a synchro-Shockley partial dislocation  
12 dipole with a three-layer spacing between the two partials (instead of the regular single-  
13 layer spacing; cf. Fig. 4) and (b) transition of a  $2H$ -type layer-stacking irregularity, to a  
14  $6H$ -type layer-stacking irregularity within the defective  $C36$  structure after the  $C14 \rightarrow$   
15  $C36$  transformation (cf. Fig. 14b); formation of the  $6H$ -type irregularity requires glide of  
16 a synchro-Shockley partial dislocation dipole with Burgers vectors of sign opposite from  
17 those of the synchro-Shockley partial dislocation dipoles which have formed the  $C36$   
18 structure to the  $C14$  structure.  
19  
20  
21  
22  
23  
24  
25  
26  
27

28 Fig. 16: Hierarchy of stacking irregularities in a  $C36$  crystal, as deduced from the results  
29 of the present XRPD and HRTEM investigations. The  $C36$  crystallite has formed from a  
30  $C14$  crystal by glide of synchro-Shockley partial dislocation dipoles. The displacement  
31 vectors between the crystal parts adjacent to the various irregularities have been  
32 indicated, including the probabilities for the displacement vectors associated with the  
33 domain boundaries for the case that the four layer-sandwich unit shift possibilities ( $X_I$ ,  
34  $X_{II}$ ,  $Y_I$ ,  $Y_{II}$ ) contribute equally.  
35  
36  
37  
38  
39  
40  
41  
42  
43  
44  
45  
46  
47  
48  
49  
50  
51  
52  
53  
54  
55  
56  
57  
58  
59  
60

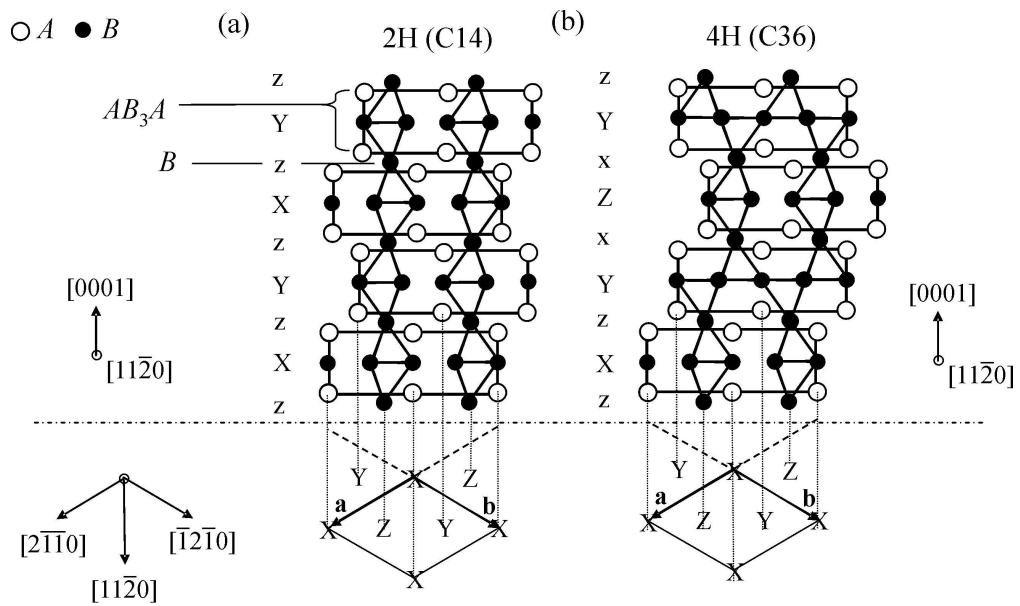


Figure 1  
222x131mm (300 x 300 DPI)

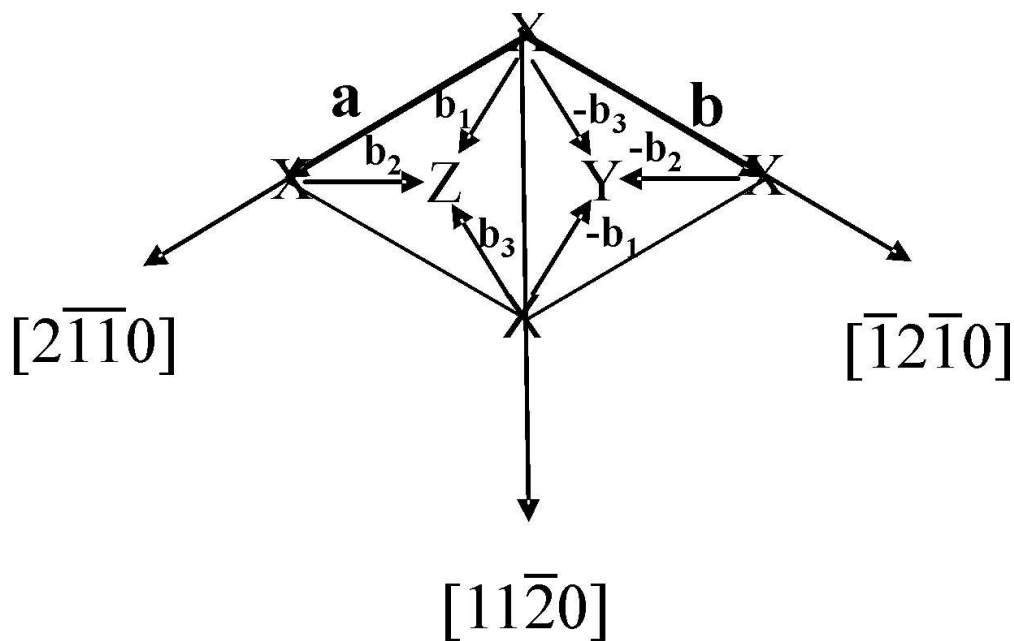


Figure 2  
104x65mm (300 x 300 DPI)

Review Only

1  
2  
3  
4  
5  
6  
7  
8  
9  
10  
11  
12  
13  
14  
15  
16  
17  
18  
19  
20  
21  
22  
23  
24  
25  
26  
27  
28  
29  
30  
31  
32  
33  
34  
35  
36  
37  
38  
39  
40  
41  
42  
43  
44  
45  
46  
47  
48  
49  
50  
51  
52  
53  
54  
55  
56  
57  
58  
59  
60

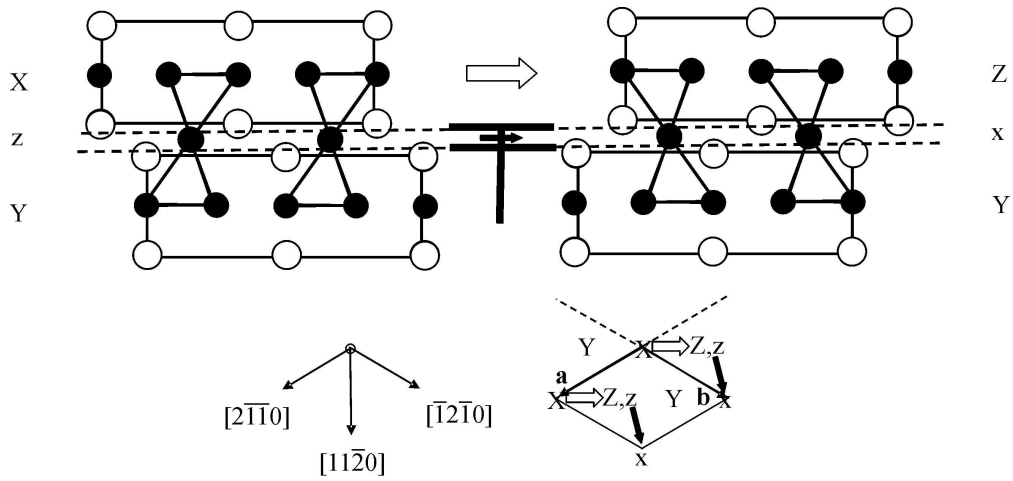


Figure 3  
223x104mm (300 x 300 DPI)

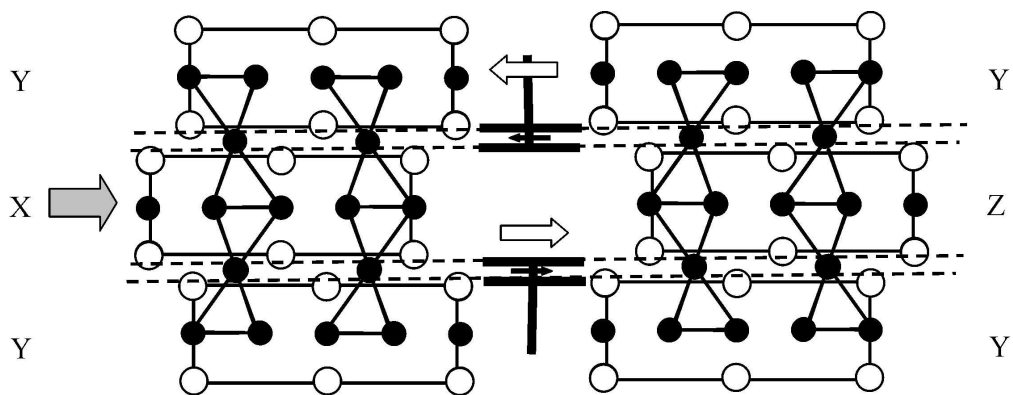


Figure 4  
189x72mm (300 x 300 DPI)

Peer Review Only

1  
2  
3  
4  
5  
6  
7  
8  
9  
10  
11  
12  
13  
14  
15  
16  
17  
18  
19  
20  
21  
22  
23  
24  
25  
26  
27  
28  
29  
30  
31  
32  
33  
34  
35  
36  
37  
38  
39  
40  
41  
42  
43  
44  
45  
46  
47  
48  
49  
50  
51  
52  
53  
54  
55  
56  
57  
58  
59  
60

1  
2  
3  
4  
5  
6  
7  
8  
9  
10  
11  
12  
13  
14  
15  
16  
17  
18  
19  
20  
21  
22  
23  
24  
25  
26  
27  
28  
29  
30  
31  
32  
33  
34  
35  
36  
37  
38  
39  
40  
41  
42  
43  
44  
45  
46  
47  
48  
49  
50  
51  
52  
53  
54  
55  
56  
57  
58  
59  
60

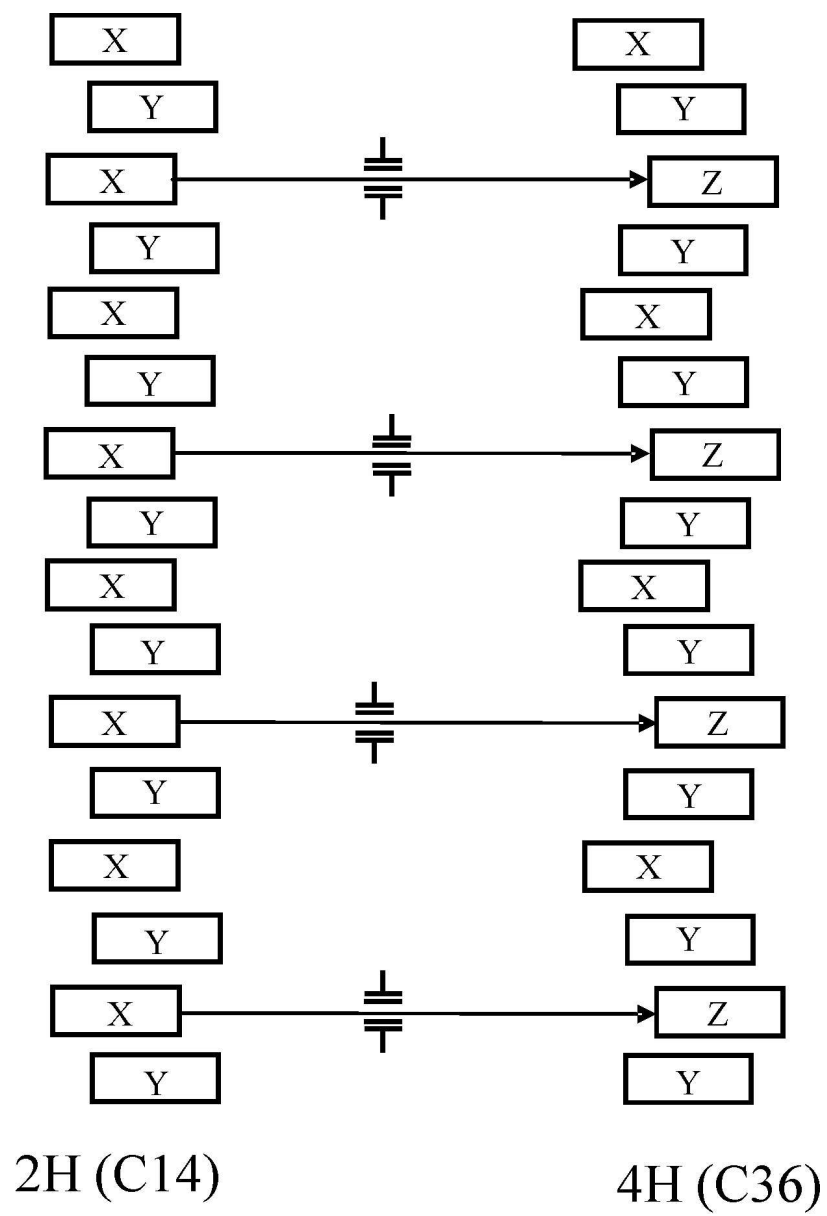


Figure 5  
104x156mm (300 x 300 DPI)

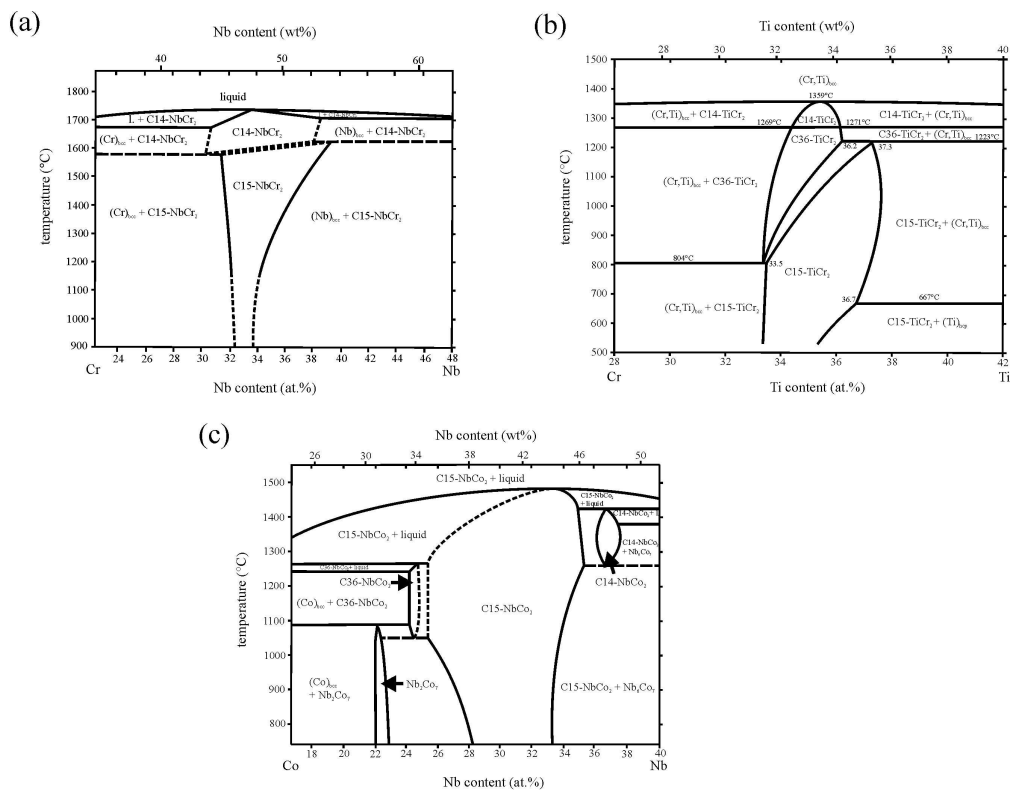


Figure 6  
225x175mm (300 x 300 DPI)

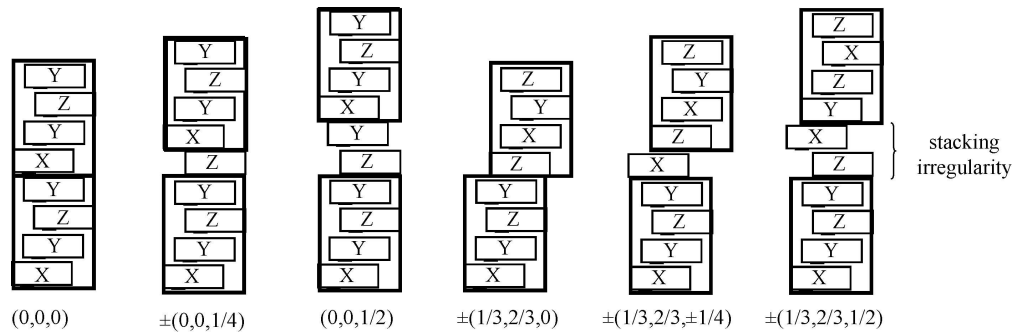


Figure 7  
237x77mm (300 x 300 DPI)

Peer Review Only

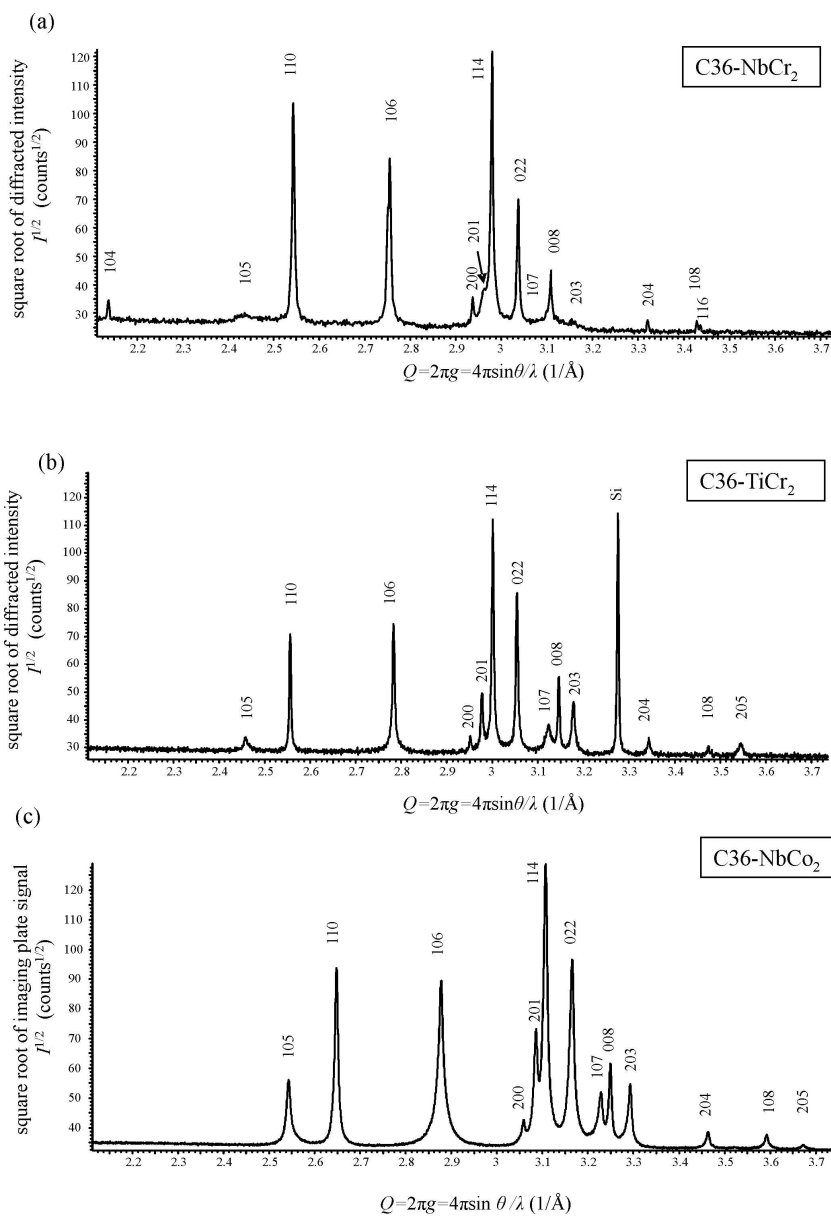


Figure 8  
176x252mm (300 x 300 DPI)

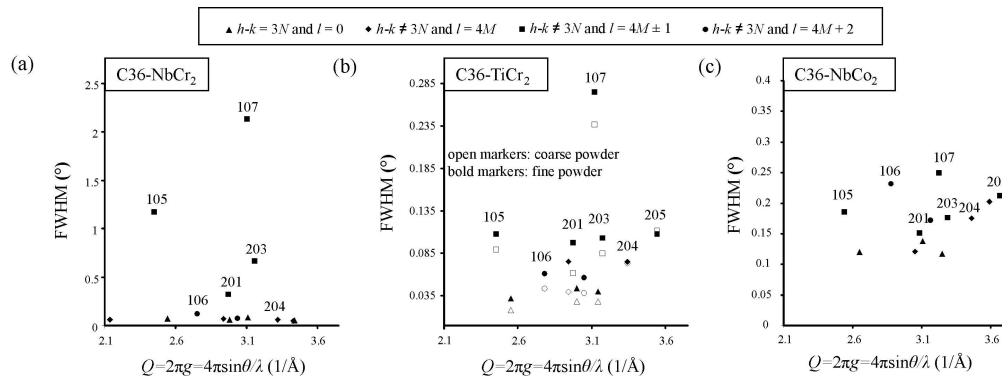


Figure 9  
244x90mm (300 x 300 DPI)

1  
2  
3  
4  
5  
6  
7  
8  
9  
10  
11  
12  
13  
14  
15  
16  
17  
18  
19  
20  
21  
22  
23  
24  
25  
26  
27  
28  
29  
30  
31  
32  
33  
34  
35  
36  
37  
38  
39  
40  
41  
42  
43  
44  
45  
46  
47  
48  
49  
50  
51  
52  
53  
54  
55  
56  
57  
58  
59  
60

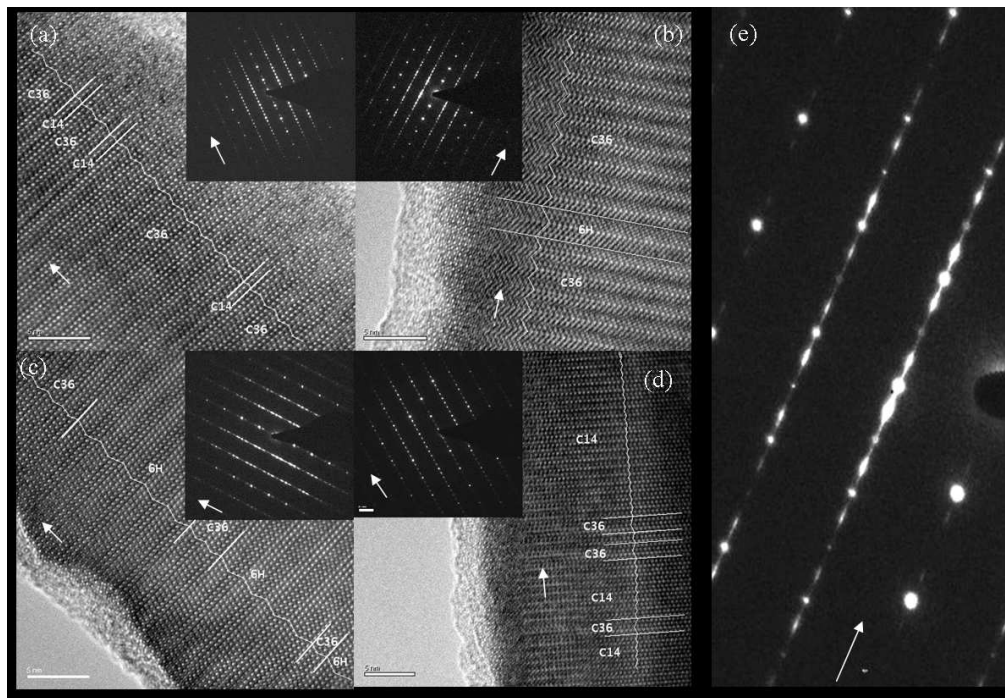


Figure 10  
199x139mm (150 x 150 DPI)

View Only

1  
2  
3  
4  
5  
6  
7  
8  
9  
10  
11  
12  
13  
14  
15  
16  
17  
18  
19  
20  
21  
22  
23  
24  
25  
26  
27  
28  
29  
30  
31  
32  
33  
34  
35  
36  
37  
38  
39  
40  
41  
42  
43  
44  
45  
46  
47  
48  
49  
50  
51  
52  
53  
54  
55  
56  
57  
58  
59  
60

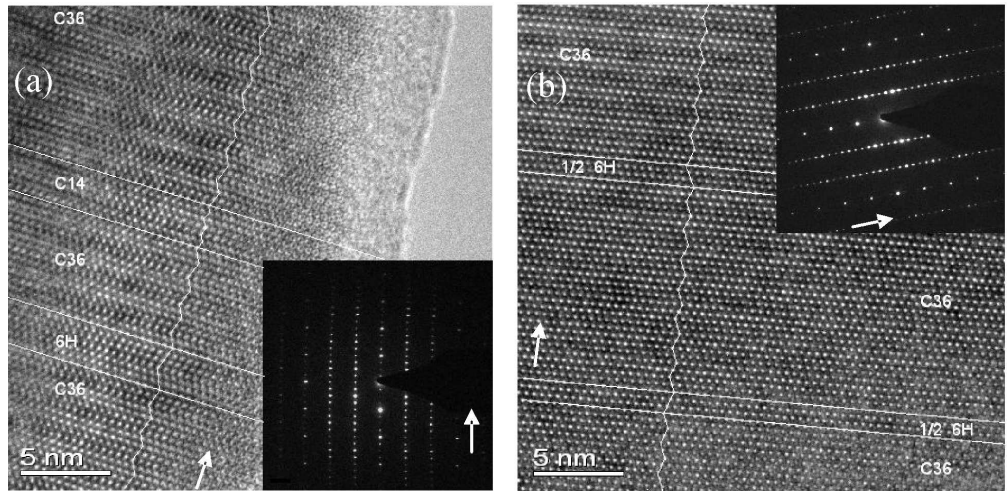


Figure 11  
164x80mm (300 x 300 DPI)

Review Only

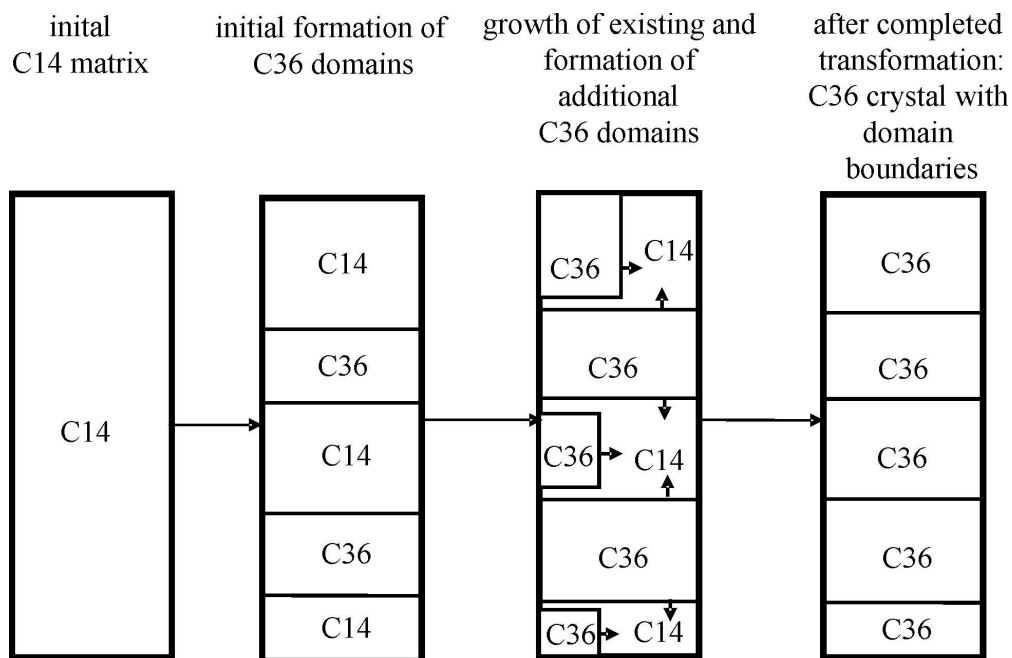


Figure 12  
164x107mm (300 x 300 DPI)

Review Only

1  
2  
3  
4  
5  
6  
7  
8  
9  
10  
11  
12  
13  
14  
15  
16  
17  
18  
19  
20  
21  
22  
23  
24  
25  
26  
27  
28  
29  
30  
31  
32  
33  
34  
35  
36  
37  
38  
39  
40  
41  
42  
43  
44  
45  
46  
47  
48  
49  
50  
51  
52  
53  
54  
55  
56  
57  
58  
59  
60

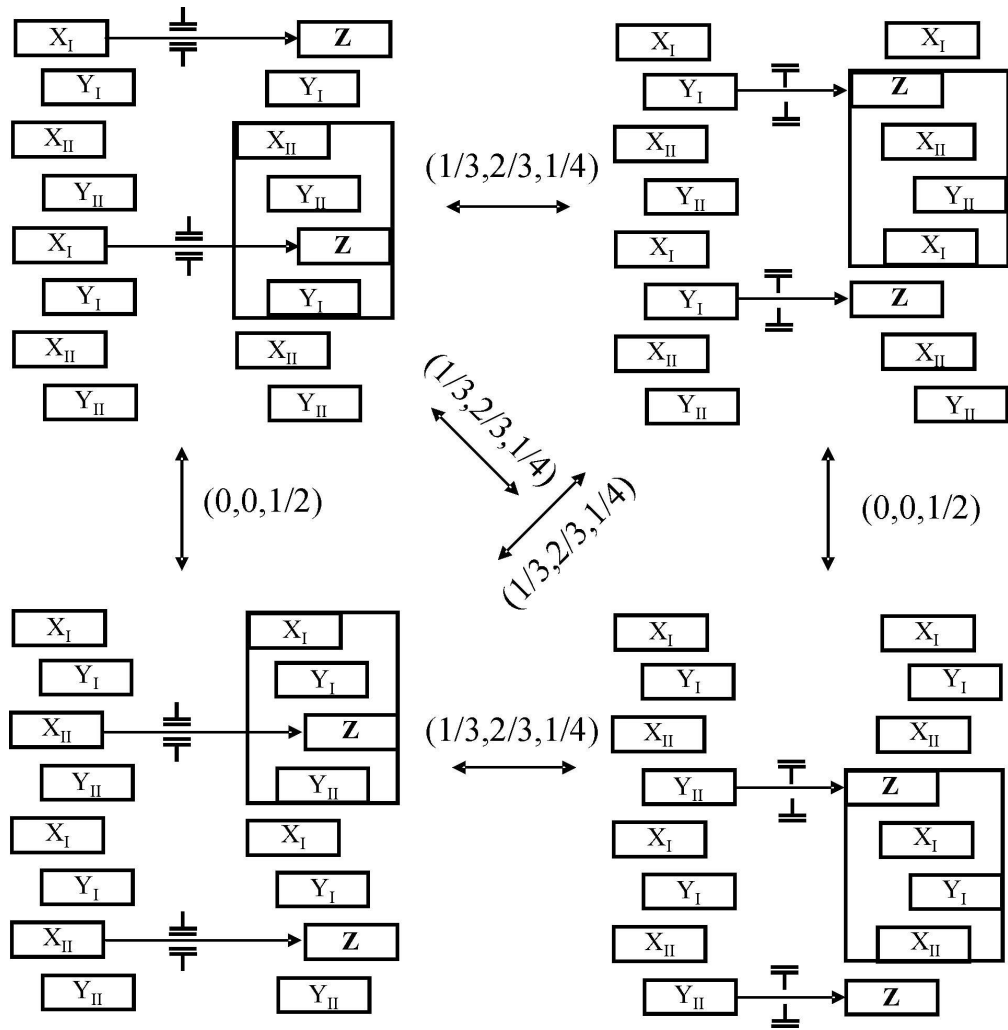


Figure 13  
162x165mm (300 x 300 DPI)

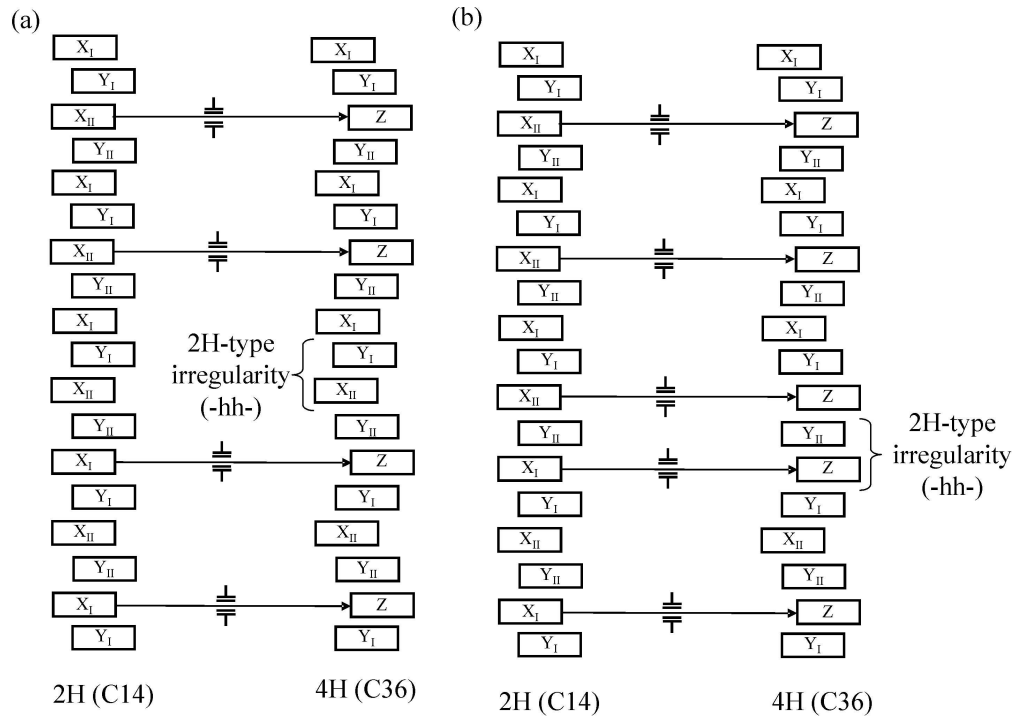


Figure 14  
242x172mm (300 x 300 DPI)

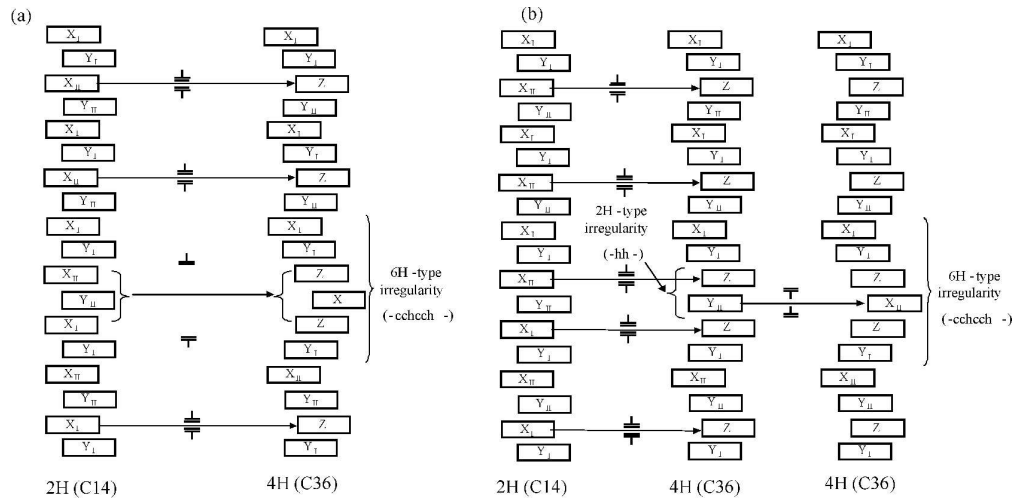


Figure 15  
283x139mm (300 x 300 DPI)

Review Only

1  
2  
3  
4  
5  
6  
7  
8  
9  
10  
11  
12  
13  
14  
15  
16  
17  
18  
19  
20  
21  
22  
23  
24  
25  
26  
27  
28  
29  
30  
31  
32  
33  
34  
35  
36  
37  
38  
39  
40  
41  
42  
43  
44  
45  
46  
47  
48  
49  
50  
51  
52  
53  
54  
55  
56  
57  
58  
59  
60

C36-crystal formed  
from C14

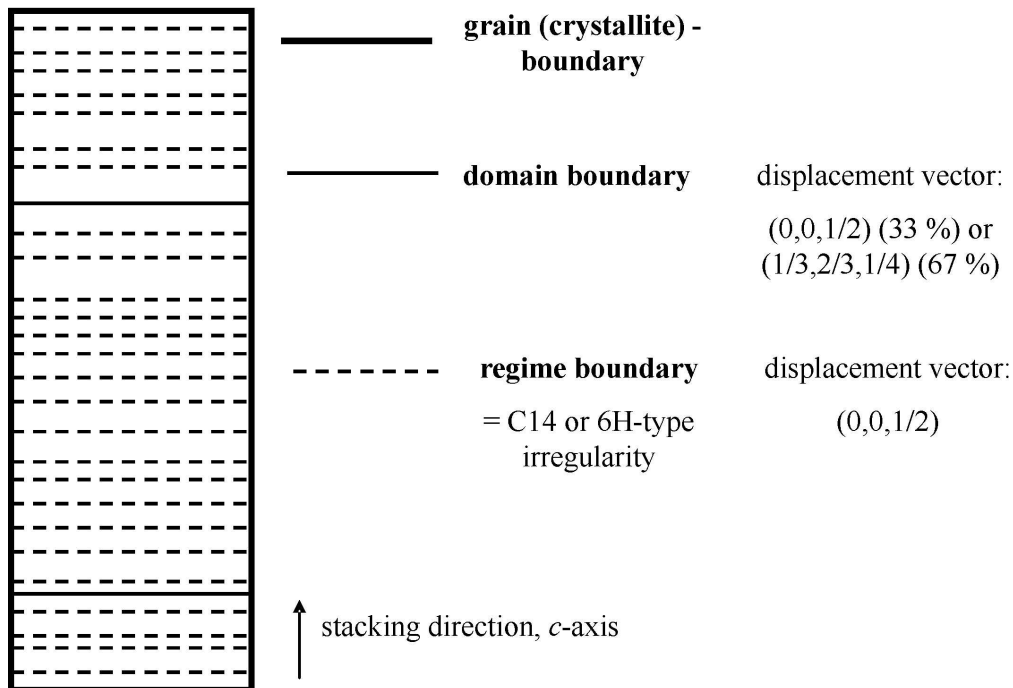


Figure 16  
179x138mm (300 x 300 DPI)

Manuscript Only